AMINE-FUNCTIONALIZED MESOPOROUS SILICA COATED CERAMICS FOR FORMALDEHYDE ADSORPTION

by

Nahid Sajia Afrin

A Thesis Submitted in Partial Fulfillment of the Requirements for the Degree of Master of Science in Nanotechnology

Examination Committee: Dr. Tanujjal Bora (Chairperson)
Dr. Supamas Danwittayakul (Co-chairperson)
Dr. Ekbordin Winijkul
Dr. Bhawat Traipattanakul

Nationality: Bangladeshi
Previous Degree: Master of Science in Chemistry
Jahangirnagar University
Bangladesh

Scholarship Donor: His Majesty the King's Scholarships (Thailand)

Asian Institute of Technology
School of Engineering and Technology
Thailand
May 2021

AUTHOR'S DECLARATION

I, Nahid Sajia Afrin, declare that the research work carried out for this thesis was in accordance with the regulations of the Asian Institute of Technology. The work presented in it are my own and has been generated by me as the result of my own original research, and if external sources were used, such sources have been cited. It is original and has not been submitted to any other institution to obtain another degree or qualification. This is a true copy of the thesis, including final revisions.

Date: 14 May 2021

Name: Nahid Sajia Afrin

Signature:

ACKNOWLEDGMENTS

Foremost, I wish to express my deepest sense of gratitude and respect to my advisor Dr. Tanujjal Bora for his indispensable guidance, constant encouragement and thoughtful suggestion throughout the whole time of my Masters. It was undoubtedly a great honor and privilege to study and work under his supervision. I will be always grateful for his untiring efforts and motivation to face the difficulties and offering the opportunity to explore the various aspects of the field of Nanotechnology. I would also be thankful for his empathy and supports during the tough time of COVID-19.

I would like to express my profound and sincere gratitude to my co-supervisor Dr. Supamas Danwittayakul for giving me the opportunity to carry out my research at MTEC, NSTDA and offering constant guidance throughout the whole time of my thesis. I am thankful for her persistent encouragement and invaluable suggestions in all the possible way to conduct the thesis work. I would also wish to thank her for being empathetic and supportive during the tough time of COVID-19.

I would like to take this opportunity to offer my profound gratitude to Dr. Ekbordin Winijkul and Dr. Bhawat Traipattanakul for being a part of my thesis committee. I am also thankful for their insightful comments and constructive suggestions on my thesis work.

I offer my genuine appreciation to the fellow members of Center of Excellence Excellence in Nanotechnology at AIT for their assistance during my research study by providing their constant motivation and suggestions.

Finally, I wish to offer special homage to my family, friends and well-wishers for all of their supports, faith, blessings, love and sacrifices throughout my studies.

ABSTRACT

Formaldehyde is one of the highly toxic indoor air pollutants emitted from the building materials, furniture coating and food preservatives, and its removal is therefore important to ensure a safe environment for us. The current study is focused on the synthesis of amine functionalized mesoporous silica coated ceramic sorbent materials to adsorb formaldehyde. The amine functionalized mesoporous silica nanoparticles was synthesized by so-gel technique from tetraethyl orthosilicate (TEOS) as silica precursor and cetyltrimethylammonium bromide (CTAB) as template. The composition of the precursor solution was modified by varying the molar ration of H_2O/TEOS and TEOS/APTES. The ceramic substrate was prepared in light casting process from micro-sized alumina particles and coated with the amine functionalized silica nanoparticles in dip coating technique. Field Emission Scanning Electron Microscopy (FESEM), Energy Dispersion X-ray Spectroscopy (EDX), Fourier transform infrared (FT-IR) spectroscopy, and N_2 adsorption–desorption isotherms were used to characterize the amine functionalized mesoporous silica nanoparticles, ceramic substrate, and the functionalized mesoporous silica coated ceramic sorbent. The adsorption efficiency of the fabricated sorbent materials was evaluated by desiccator method and the equilibrium characteristics were evaluated by using Langmuir adsorption isotherm. The sample synthesized with H_2O/TEOS = 45.5 and TEOS/APTES = 80/20 showed highest adsorption capacity because of its specific surface area, pore diameter and amine groups.

CONTENTS

LIST OF TABLES

LIST OF FIGURES

LIST OF ABBREVIATIONS

AMPS	= Amine Functionalized Mesoporous Silica
APTES	= (3-Aminopropyl)triethoxysilane
AEAP	= n-(2-amino-ethyl)-3-amino-propyltrimethoxysilane
AEEA	= 3-(2-(2-amino-ehtylamino)ethylamino) propyltrimethoxysilane
BET	= Brunauer–Emmett–Teller
CTAB	= Cetyl Dodecyl Ammonium Bromide
EDX	= Energy Dispersion X-ray Spectroscopy
EtOH	= Ethanol
EPA	= Environmental protection Agency
FT-IR	= Fourier Transform Infrared
HDDA	= 1,6-Hexanedioldiacrylate
H_2O	= Water
IDLH	= Immediately Dangerous to Life and Health
MPS	= Mesoporous Silica
MSN	= Mesoporous Silica Nanoparticles
MBS	= Metabisulfite
µm	= Micrometer
nm	=Nanometer
NIOSH	= National Institute for Occupational Safety and Health
NaOH	= Sodium Hydroxide
NH_3	= Ammonia
OSHA	= Occupational Safety and Health Administration
POE	= Phenoxyethanol
PDC	= Polymer Derived Ceramics
SEM	= Scanning Electron Microscopy
TEOS	= Tetraethyl orthosilicate
TEM	= Transmission Electron Microscopy
UV	= Ultraviolet
VOCs	= Volatile Organic Compounds

CHAPTER 1
INTRODUCTION

1.1 Background of the Study

Formaldehyde is one of the most common volatile organic compounds (VOCs). It is a colorless gas and possesses a sharp pungent odor. Formaldehyde is considered as one of the highly toxic VOCs and can cause serious health hazard. Despite being a toxic pollutant, formaldehyde is used widely in different industrial sectors, such as building materials, textile industry, particle board, household products, glues, wood industry, automobile sector, etc.

The easy availability, high reactivity and lower cost of this chemical substance makes it a suitable candidate to be used in the industrial sectors. Wood, furniture and building manufacturing industries uses formaldehyde as varnishes and paints from which the gas is emitted to the indoor air (Gürü et al., 2006; Halvarsson et al., 2008; Kim, 2009). Tobacco smoking (Leaderer & Hammond, 1991), combustion or burning of wood, can also introduce formaldehyde to the atmosphere. Human and other metabolic organisms introduce a very little amount of formaldehyde to the environment due to their metabolic activities. Different indoor and outdoor formaldehyde sources are shown in Figure 1.1.

Aqueous solution of formaldehyde is known as formalin which contains 40% of formaldehyde by volume (37% by weight) and 6-13% methanol by volume in water (OSHA Fact Sheet: Formaldehyde | Occupational Safety and Health Administration, n.d.). It is used as preservative in the medical sector as well as in the food industries; formalin from the preserved food and medicine can be diffused to the atmosphere and cause indoor air pollution. Formaldehyde is also used as disinfectants, germicides, and fungicides in different industries.

If inhaled, formaldehyde can cause severe breathing problem, nausea and burning sensation in throat, eye, and nose (Ewlad-Ahmed et al., 2012). Exposure to low level (0.5 ppm) of formaldehyde for a long period of time can cause respiratory problems (like asthma) as well as skin diseases (for example itching, irritation or dermatitis).

According to the National Institute for Occupational Safety and Health (NIOSH) 20 ppm of formaldehyde is considered to be immediately dangerous to life and health (IDLH) (OSHA Fact Sheet: Formaldehyde | Occupational Safety and Health Administration, n.d.). In different laboratory tests, it has been established that the exposure to formaldehyde can cause cancer in animals. According to Environmental protection Agency (EPA), formaldehyde is one of the probable human carcinogens. The National Cancer Institute has reported that the exposure to formaldehyde can cause leukemia in humans (Formaldehyde and Cancer Risk - National Cancer Institute, n.d.). According to US EPA, the permissible formaldehyde limit in the indoor air is 0.1 ppm which can protect any individual from both irritation as well as cancer hazards (Golden, 2011). According to OSHA, the permissible exposure limits (PELs) of formaldehyde in air is 1 ppm for 8 hours and 2 ppm for 15 mins(*OSHA Rulemaking on Formaldehyde Exposure Limits | Occupational Safety and Health Administration*, n.d.).

Figure 1.1

Sources of Formaldehyde in the Indoor Atmosphere

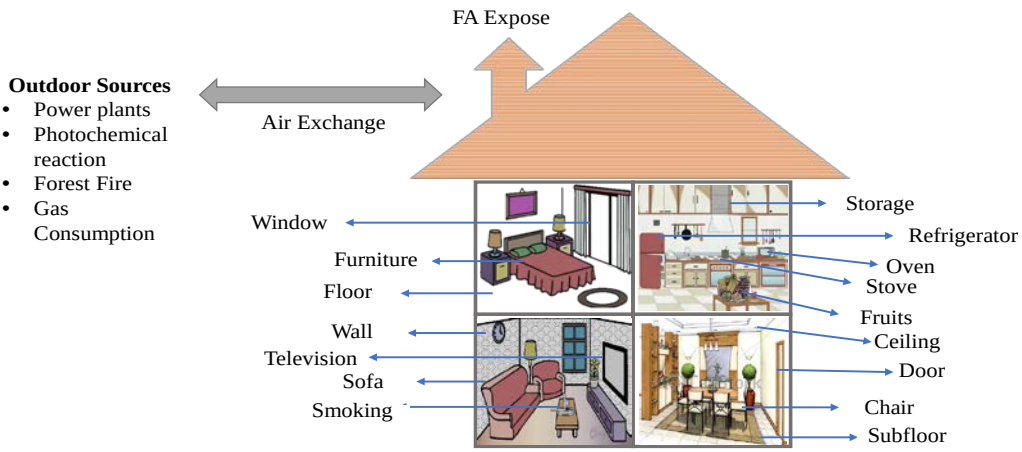

The concentration of formaldehyde in indoor air is generally 2-10 times higher than that of the outdoor air, as furniture and building materials are the main source of formaldehyde emission (Báez et al., 2003; Marchand et al., 2006). In 2009, Ongwandee et al. (Ongwandee et al., 2009) have estimated the concentrations of formaldehyde in 12 office building in Bangkok and reported an average concentration of formaldehyde

in the indoor air as 35.5 µg/m3 (0.04 ppm), while the concentration of the outdoor air was 10.1 µg/m3 (0.01 ppm).

1.2 Statement of the Problem

The removal of formaldehyde from the indoor environment is highly required to protect living organisms from severe health hazards. Removal of gaseous formaldehyde was attempted before by using activated carbon, potassium permanganate or aluminum oxide (Ewlad-Ahmed et al., 2012). However, these materials undergo different kinds of reactions with other VOCs present in the atmosphere which limit the adsorption capacity of these materials.

Glass fibers were also used for the removal of formaldehyde from the atmosphere (Gesser, 1984). Polyethylene hydrazine and amines were sprayed on to the fibers for the formaldehyde adsorption. However, the method was not successful because it offered a short time solution.

Activated carbon and Tenax TA (a 2,6-Diphenylene oxide based porous polymer resin produced by Buchem BV) have been developed for the removal of VOCs from the indoor environment and they are considered as highly suitable for the removal of VOCs from the environment. However, these materials have shown less suitability for the removal of formaldehyde vapor. Additionally, clogging of pore and difficulty in regeneration of the materials are problems of activated carbon-based adsorbent materials (Ewlad-Ahmed et al., 2012).

Mesoporous silica based adsorbent materials (Stein, 2003) were studied for the removal of formaldehyde(Srisuda & Virote, 2008), but studies on the practical applications and efficiency to remove formaldehyde using this mesoporous silica based adsorbent materials is still limited (Hartmann & Bischof, 1999, 1999; Idris et al., 2010; Kosuge et al., 2007; Matsumoto et al., 2004; Ueno et al., 2002). Moreover, studies on the adsorption efficiency of mesoporous silica coated ceramic based adsorbent have not been carried out yet.

Nevertheless, preparation methodologies of some of the adsorbents is very complex and sometimes require expensive materials. All these aspects make the fabrication

techniques inconvenient and costly. Mesoporous silica coated porous ceramic substrates, in this regard, can be a simple and cost-effective solution for the adsorption and removal of formaldehyde. Moreover, the functionalized mesoporous silica nanoparticles will offer desired high specific surface area and functionality required for the effective adsorption of formaldehyde and its subsequent removal.

1.3 Objectives of the Study

The overall objective of this study is to synthesize amine functionalized mesoporous silica nanoparticle coated ceramic substrate for the efficient removal of formaldehyde vapor. The specific objectives of the study are as follows:

1. To synthesize amine functionalized mesoporous silica nanoparticles.
2. To synthesize alumina ceramic substrate and coat them with amine functionalized mesoporous silica.
3. To evaluate the performance of the amine functionalized mesoporous silica coated ceramic substrate towards the adsorption and removal of formaldehyde vapor.

1.4 Scope of the Study

The formaldehyde adsorbents have wide range of application in various industries, including textile industries, paint industries, food industries, automobile sectors, and so on. Formaldehyde exposed from the household sources including stove, smoke, paint, carpet, food preservatives, etc. Thus, the sorbent materials have huge application where carcinogenic formaldehyde gas is exposed. The current research focuses on the preparation of amine functionalized mesoporous silica coated ceramic sorbents to adsorb and remove formaldehyde vapor from air.

1.5 Limitation of the Study

- Only micro- and nano-sized alumina are used to prepare porous ceramic substrates, and other types of ceramics are not considered.
- Only mesoporous silica nanoparticles are considered for the coating of the ceramic substrates; other types of nanoparticles are not considered.
- The research is limited to the adsorption and removal of formaldehyde only, other types of VOCs are not considered.

CHAPTER 2
LITERATURE REVIEW

Formaldehyde is one of the most toxic VOCs present in the environment. It is highly reactive and flammable at room temperature. In ambient condition, formaldehyde quickly oxidized to carbon dioxide in presence of light and to formic acid by reacting with hydroxyl radicals (Kaden et al., 2010a). Formaldehyde is formed primarily by numerous anthropogenic activities as well as natural sources (Kaden et al., 2010a).
The toxic formaldehyde gas is released in the environment by the combustion or decomposition of biomass and from volcanoes as well. Moreover, formaldehyde is produced extensively in the industries as fixative and disinfectant, or as a preservative for the consumer products. All of these products and their usage is the most common sources of formaldehyde in the indoor atmosphere. Formaldehyde can be indirectly exposed to the indoor air by the oxidation of the other VOCs and the reaction between alkene containing terpenes and ozone in the outdoor environment which can enter the indoor atmosphere by the exchange of air (Kaden et al., 2010b).

2.1 Formaldehyde Toxicity

The most important industrial chemical, formaldehyde, also plays an important role in the biological system. Formaldehyde acts as an intermediate in the cellular metabolism and plays essential role for the biosynthesis of thymidine, purine and other certain amino acids (Kaden et al., 2010a). Exposure of human and animals to this chemical results in metabolic incorporation of formaldehyde into DNA, RNA, and proteins. Formaldehyde molecules bind covalently with the macromolecules and results in toxic effects in human and animals (Heck et al., 1990). Formaldehyde causes irritation in the respiratory tract by metabolizing in the nasal mucosa and reacting covalently with nucleic acids and proteins.

Short time exposure to formaldehyde has been found to cause cytotoxicity, while relatively long-time exposure results in carcinogenicity. When animals and humans are exposed to the environment containing formaldehyde vapor, it affects their breeding capability and life span as well (Duong et al., 2011). Formaldehyde not only affects human and animals adversely, it also affects the plant species as well. The most

significant effect of formaldehyde on plant species is the reduction of water content and wet weight of the plant (Teiri et al., 2018).

2.2 Techniques to Remove Formaldehyde

Formaldehyde can be removed by both physical and chemical methods, for example, adsorption, scrubbing and advanced oxidation (Bum An et al., 2012). Sometimes both physical and chemical methods are employed together to remove formaldehyde from the atmosphere. Among the formaldehyde removal techniques, adsorption and scrubbing are the physical techniques, while oxidation is the chemical technique.

Oxidation is the chemical process where formaldehyde is removed from the indoor air by chemical reaction. Oxidation usually requires high temperature and suitable environment, whereas the catalytic oxidation is carried out at ambient atmosphere. The most active catalytic oxidation technique uses Pt/ TiO_2 (Huang et al., 2013). On the other hand, scrubbing is the physical method where sodium metabisulfite (MBS)-assisted water scrubbing is carried out to remove dilute formaldehyde from the resin production plants (Prado et al., n.d.). However, the most common and efficient method for the removal of formaldehyde from indoor air is the adsorption technique. Several materials have been developed as sorbent material which can efficiently adsorb and remove formaldehyde from the indoor air.

2.3 Sorbent Materials for the Removal of Formaldehyde

Adsorption is the most common and efficient technique used to remove formaldehyde from the indoor atmosphere. This physical technique includes several sorbent materials to adsorb formaldehyde from the atmosphere. Some example of such sorbent materials is activated carbon (Bum An et al., 2012), mesoporous silica (Ewlad-Ahmed et al., 2012) and porous metal-oxides (Krishnamurthy et al., 2018a).

Activated carbon has been extensively used to remove formaldehyde by adsorption from the indoor environment. Despite showing excellent VOC removal capacity, activated carbon lacks efficiency for the adsorption and removal of polar materials, like formaldehyde (Bum An et al., 2012). Mixed metal oxide is another class of compound that is employed for the adsorption of formaldehyde. Typically, metal oxides used for the adsorption includes TiO_2/SiO_2, ZrO_2/SiO_2 etc (Krishnamurthy et al., 2018b). In

some cases, transition metal oxide supported metal catalysts are used for the removal of formaldehyde. Usually, the transition metal oxides include Fe_2O_3, Al_2O_3, CeO_2, ZrO_2, MnO_2, Co_3O_4, NiO, and TiO_2 and the metal catalysts include Ag, Au, Pt, Pd, Rh, and Ru (Tan et al., 2019). Mesoporous silica is also a most widely known class of compound that has been used for the adsorption and removal of formaldehyde.

2.3.1 Porous Sorbent Materials

Porous materials typically contain matrix and fluids. The matrix constitutes the frame of the materials; fluid can be either liquid or gas. Porous materials are characterized by their high specific surface area, low density, and number of novel and unique properties in different fields (Nishiyabu, 2012).

Depending on the size of the pores, porous ceramics can be categorized into three different classes (Liu & Chen, 2014); such as,

- Microporous materials, pore sizes less than 2 nm
- Mesoporous materials, pore sizes of around 2-50 nm
- Macroporous materials, pore sizes more than 50 nm

Figure 2.1

Microstructure of Porous Gypsum at Meso and Micro Scale

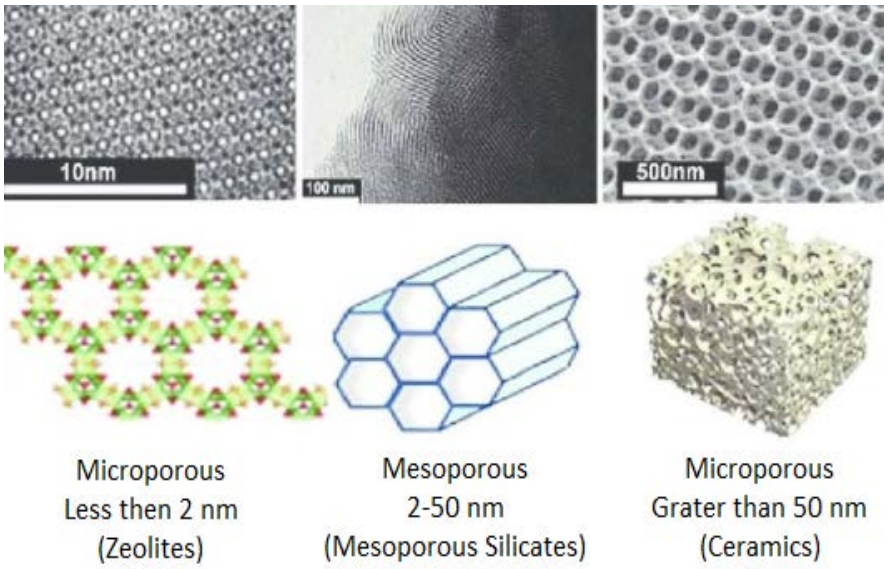

Among the three class of nanomaterials, mesoporous nanomaterials which has pore dimension in the range of 2 nm to 50 nm is most widely utilized in different application for their unique properties. However, the rules about using porous materials varies from country to country, thus the classification based on porosity is not adopted worldwide.

The pores of porous materials are also classified as open pores or closed pores depending on their accessibility to the surrounding environment. Open pores allow the molecules to access the surrounding medium. Open pores are also categorized as open at both the ends and open at one end. On the other hand, closed pores prevent the access of molecules from the surrounding medium. According to Ruike et al. closed pores are those that are not accessible by Helium gas at 303 K temperature (Zdravkov et al., 2007).

Figure 2.2

Classification of Pores (a) Closed Pore; b and f: Pores Open at One End; c, d and g: Open Pores; e: Pores Open at Both Ends(Rouquerol et al., 1994)

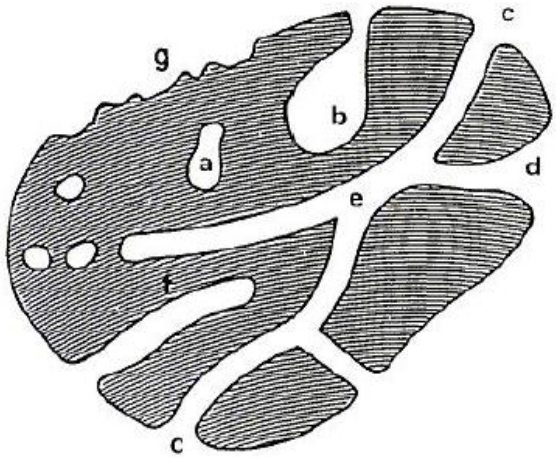

2.4 Silica Nanoparticles

Nanomaterials are those compounds which has at least one dimension in the nanometer range (1-100 nm). This materials can be classified as zero-dimensional (0D), one-dimensional (1D), two-dimensional (2D), and three-dimensional (3D) nanomaterials (Fadeel & Garcia-Bennett, 2010).

Zero dimensional nanomaterials are those where all three dimensions are confined in the nanometer range, i.e., within 1-100nm range. Quantum dots are example of this class of compounds. Amorphous, crystalline, polymeric, ceramic and metallic compounds can be known as zero dimensional materials. One dimensional (1D) nanomaterials are those which has at least one dimension in the nanometer range. Nanotube, nanowires, nanofibers and nanorods fall in this class. Two dimensional (2D) materials are known to have two dimensions in the nanometer range. Nanofilms, nanocoating, nanolayers are known as two dimensional. Lastly, three dimensional (3D) nanomaterials are those where none of the dimensions fall in the nanometer range. These class compounds are also known as bulk materials ("Nanomaterials Definition Matters," 2019).

Silica nanoparticles used in different applications can be categorized into two classes: porous and nonporous particles. Porous particles basically fall in the mesoporous class. Both nonporous and porous silica nanoparticles are amorphous in nature. The porosity, size and shape of the pores of porous nanoparticles can be controlled by varying the synthesizing condition, for example, surfactant, pH, temperature etc.

2.4.1 Porous Silica Nanoparticles

Although porous silica nanoparticles basically fall in the mesoporous class, but in general, depending on the size of the pores, the three class of silica nanoparticles are microporous silica nanomaterials, mesoporous silica nanomaterials and macroporous silica nanomaterials.

Mesoporous silica nanoparticles fall in the dimension range of 2 nm to 50 nm. They can be classified into two major classes: M41S Type mesoporous nanoparticles, hollow mesoporous silica nanoparticles, and Originally modified silica (ORMOSIL) nanoparticles (Feng et al., 2016).

Figure 2.3

Mesoporous Silica a) M41S-Type, b) ORMOSIL-Type, c) Hollow-Type Mesoporous Silica Nanoparticles

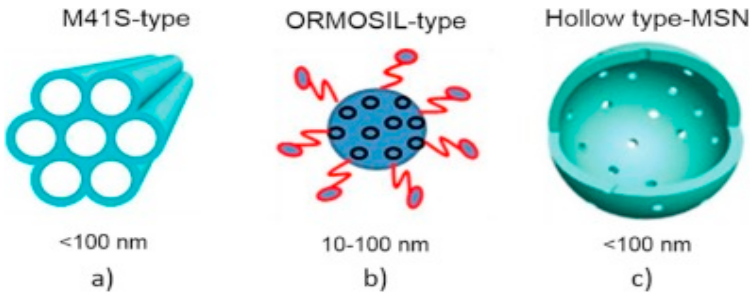

2.4.2 Synthesis of Silica Nanoparticles

Silica nanoparticles can be synthesized in two ways: sol-gel method and microemulsion method (Zou et al., 2008).

a. In sol-gel method (Greasley et al., 2016), spherical, monodispersed silica nanoparticles can be prepared. The hydrolysis of alcoholic dilute solution of TEOS (in ethanol) is carried out to produce the silica nanoparticles. pH has great impact on the size of the nanoparticles. This method is usually carried out at a very high pH. The size of the nanoparticles can vary from 10 nm to 2 µm depending on the synthesizing condition. Hydrolysis and condensation reaction occur during the synthesis of silica nanoparticle in this method, which can be shown as follows:

   Hydrolysis: $Si\text{-}(OR)_4 + H_2O \rightarrow Si\text{-}(OR)_3\text{-}OH + R\text{-}OH$

   Condensation: $Si\text{-}(OR)_3\text{-}OH + HO\text{-}Si\text{-}(OR)_3 \rightarrow [(OR)_3Si\text{-}O\text{-}Si(OR)_3] + H\text{-}O\text{-}H$

b. In microemulsion method (Greasley et al., 2016) hydrolysis of TEOS in inverse microemulsion is carried out in controlled manner. In this method, inverse micelle is formed in presence of surfactant in nonpolar solvent. The formation of inverse micelle initiates the formation of silica nanoparticles.

2.4.2.1 Synthesis of Porous Silica Nanoparticles

Porous silica nanomaterials belong to the molecular sieve family. Among all classes of porous silica nanomaterials, mesoporous silica is most widely used due to their enhanced unique properties for different applications. Some of the properties include controllable porosity, particle size, morphology, and chemical stability (Mehmood, 2017).

In order to synthesis mesoporous silica nanoparticles, cationic surfactant molecules are used to initiate the process. Surfactants form micelles which act as a template to produce desired sized particles with anticipated porosity. After the formation of particles with desired size and porosity, the samples are calcined to remove the surfactant template. The mechanism for the formation of mesoporous silica nanoparticles is shown in figure-2.4.

Cai et al. reported the successful formation of mesoporous nanomaterial, MCM-41 (Cai et al., 2001). In this process at first surfactant molecules (Usually CTAB) in added to the water and alcohol mixture at high pH under stirring which produces micelles. Then TEOS is added to the mixture under stirring. After the completion of the reaction the sample was calcined at high temperature to remove the template. This gives the mesoporous nanoparticle with desired porosity and particle size. Concentration of silica and surfactant plays important role to control the particle size. The particle size can be controlled by varying the ratio of silica and surfactant molecules (Lin et al., 2012). A different way of achieving mesoporous silica nanomaterials was reported by Mann et al. According to his study the mesoporous interior can be formed by hydrolysis and condensation reaction of TEOS (Fowler et al., 2001).

Figure 2.4

Schematic Diagram for the Formation of Mesoporous Silica Nanoparticles(Yang et al., 2012)

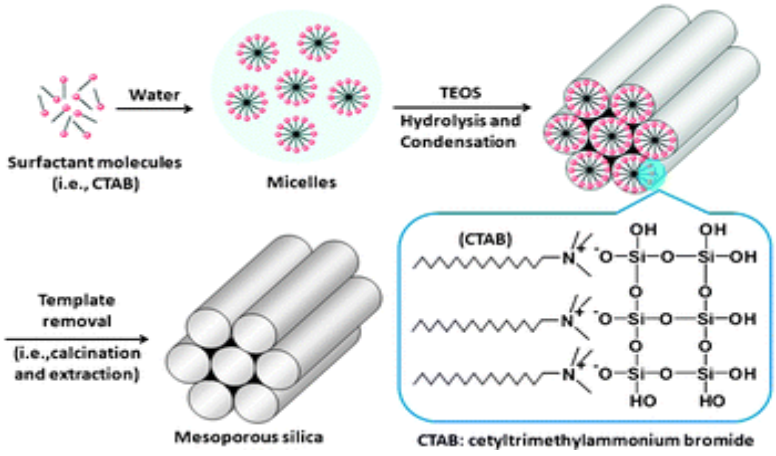

Morphological and textural features of mesoporous silica nanoparticles vary widely depending on the composition ratio of the precursor solution. Different synthesizing methodology and structural features of mesoporous silica MCM-41 is summarized in table 2.1.

Table 2.1

Review on Synthesizing Methodology and Structural Features of Mesoporous Silica MCM-41

Synthesis composition	Specific Surface Area, (m^2/g)	Particle Size (nm)	Pore Diameter (nm)	References
TEOS:AEEA:CTAB: EtOH:H_2O = 0.85:0.15:0.22:5:80	141.40		159.8	(Srisuda & Virote, 2008)
TEOS:CTAB:NaOH: H_2O = 1:0.1:0.30:60	871	-	2.61	(Chen & Wang, 2002)
TMOS:CTAB: Methyamine:H_2O = 1:0.215:2:120	992	-	3.32	(Trouvé, Batonneau-Gener, Valange, Bonne, & Mignard, 2012)
TEOS:CTAB:NH_3: H_2O:C_2H_5OH = 1:0.3:11:144:58	-	806.5	-	(Dahane et al., 2016)
TEOS:CTAB: NH_3:H_2O	1460	-	2.1	(Meléndez-Ortiz et al., 2012)
TEOS:NaOH: CTAT:F68 = 1:0.53:0.011:0.0037	468	1.94	1500	(Brigante & Avena, 2014)
TEOS:CTAB:NH_3: C_2H_5OH:H_2O = 1:0.2:21:50:475	978	-	-	(Kirik, Parfenov, & Zharkov, 2014)

2.4.3 Surface Modification of Silica Nanoparticles

Silica nanoparticles have been used in various sectors, such as insulators (Maszara et al., 1988), nanocomposites (Harmer et al., 1996; Kang et al., 2016), coating, catalysis (Amgoune et al., 2008; Obrey & Barron, 2002), film substrate (Grosso et al., 2002), Biomaterials (Gutwein & Webster, 2004; Smitha et al., 2007) etc. However, these applications of silica nanoparticles require surface modification, because the surface properties control the function of silica nanoparticles (Kang et al., 2016). The surface of silica nanoparticle can be modified through two pathways: physical modification and chemical modification (Kang et al., 2016).

a. Physical Surface Modification Method: In this method, surface modification is achieved by adsorbing macromolecules or surfactant silica nanoparticle surface. Surfactant's molecules get attached to the surface of silica nanomaterials with hydrophilic group through electrostatic interaction.
b. Chemical Surface Modification Method: In this method, modifier agents or grafting polymers are used for the surface modification. Due to the strong interaction between surface modifier and the silica nanoparticles the chemical modification method is most widely used.

Silanes have hydrolyzing group and organofunctional ends which makes them suitable as surface modifying agents. Silanes are used for the coupling of silica nanomaterials on the surface of the matrix. General structure of coupling agents is $RSiX_3$, where X represents the hydrolyzing group, such as methoxy, ethoxy, chloro, etc and R represents the organic group having different functional group for different functionality. The silica surface contains hydroxyl group (-OH) which reacts with the hydrolyzing group (X).

To modify the surface of the silica nanoparticles, organoalkoxysilane or halosilane can be used which forms bond with the silanol group present at the surface of the silica nanoparticles through condensation reaction. Surface modification can also be carried out by using different types of organosilanes, such as MPTS, APTES and some other PEG (Kang et al., 2016).

Silica nanoparticles achieve unique and desirable properties through surface modification. PEGMA and PPGMA was used to improve the dispersion property of

silica nanoparticles (Vickers, 2017). TEOS was used to modify the surface of silica nanoparticles in Stöber method where TEOS was hydrolysis reaction was carried out to get the modified surface. The functionality of silica surface can also be improved via incorporation of the reactive groups, such as VTES. Surface of the silica nanoparticles was grafted with PPG or PEG through UV-photopolymerization after reacting with VTES. The surface modified silica nanoparticles showed high weight loss and low zeta potential.

Cationic surfactants was used by Xiao-Kun Ma et al. to produce highly dispersed silica nanoparticles (Ma et al., 2010). In this method CTAB was used as a cationic surfactant molecule which was adsorbed on the surface by interacting with the negative hydroxyl group (anionic) present on the surface of the silica nanoparticles. These adsorption decreases the surface energy of the silica nanoparticles and this increases the spatial atomic arrangement. The modification of silica surface in this case produced monodispersed particles with enhanced stability (Ma et al., 2010).

Silica surface modification through hydrophilic polymer was carried out by Tae Park et al (Park et al., 2010). They have mentioned different methods of polymer chain attachment to the surface of silica nanoparticles in their work. In one method, they have modified the surface using a three-step process where the polar polymer, such as PSSA and POEM were grafted to the surface of the silica nanoparticles. The dispersion behavior was enhanced by this process.

Sonyeon Kim et at. Showed the modification of the surface through graft polymerization by using MMA (Kim et al., 2004). The grafting was carried out under UV irradiation. Z. Lou et al. showed surface modification by introducing functionality on the surface of silica nanoparticles. In this is one step process, TEOS was hydrolyzed in polar and aqueous solution in presence of MPMS. This process introduces organic functional group of the silica surface which prevents the agglomeration of silica nanoparticles. Marini et al. synthesized surface modified silica nanoparticles having core-shell structure from TEOS and then surface modification was carried out using VTEOS (Alam & Al Riyami, 2018). They had reported that the modified silica nanoparticles showed high carbon content in the shell and core containing oxygen and

silicon. In another study, Wang et al. reported the modification of surface of the silica nanoparticles by in covalent and no-covalent method (Wang et al., 2014).

2.5 Ceramic Substrate as Matrix

Ceramic is the class of compounds that is widely used in laboratories and industries due to their stability, heat resistance, hardness, chemical inertness, and biocompatibility (Ebnesajjad, 2014). Ceramics are basically non-metallic inorganic solid materials made up of metallic or non-metallic compounds whose shape and hardness are achieved by heating at high temperature. Depending on the chemical and crystal structure, ceramics are classified as oxide ceramics, chalcogenide ceramics, Nitride and oxynitride ceramics, carbide and borides (Ebnesajjad, 2014). Among all these types of ceramics the most dominant class is the oxide ceramics. Oxide ceramics possesses chemical stability and refractory character at very high temperature in the oxygen containing environment.

Stretching, bending, melting, wear and corrosion resistance property of ceramic makes it an ideal candidate as matrix. A variation in these properties is observed depending on the chemical structure of ceramic materials. Alumina ceramic (Al_2O_3), mullite ($3Al_2O_3.2SiO_2$), zirconia ceramic (ZrO_2), silicon carbide (SiC), Steatite Ceramics (Mg_2SiO_4), etc. are such types of ceramic materials. Different ceramic materials can be used for different purpose depending on their corresponding properties. For examples, Alumina possesses high thermal stability, wear and corrosive resistance; Steatite shows high insulating properties and can be suitable for electronic devices; Zirconia ceramics has very high strength and toughness in the atmospheric condition; Mullite possesses low thermal expansion and thermal conductivity, excellent resistance to creep, high chemical stability and high temperature strength (Ebnesajjad, 2014).

2.5.1 Ceramic Substrate for the Adsorption of Volatile Organic Substance

Adsorption of VOCs on the ceramic substrate can be done by the modification of the ceramic structure, such as introducing high porosity to the structure. Introduction of porosity in the structure enhances the surface area where the VOCs can be trapped. Porous materials are made up of continuous solid phase that forms the basic porous frame and a fluid phase that forms the pores in the solid. The fluid phase can consist of gas or liquid when there is a gaseous medium or liquid medium in the pore, respectively.

However, all the materials with pore do not referred to as porous materials. For example, defects, such as, holes and crannies, in the solid lowers the material's performance. These materials will not be considered as porous. For a material to be considered as porous, it must possess two important characteristics: first one is that the material should contain a lot of pore and the second one is that the pore should be designed in such a way that they can achieve the expectant index in terms of the performance of a material. Therefore, the pore of porous materials can be considered as functional phase and may offer optimizing action to the material's performance.

Porous ceramics are those which have high percentage of porosity, usually 20 to 95% (Liu & Chen, 2014). These materials typically composed of the solid ceramic phase and the gas-filled porous phase. The gas content of the pores can be exchanged with the environment through the pore channels. However, the closed pores may contain a gaseous composition which is independent of the environment (Al-Naib, 2018).

Expansive research has been done on the porous ceramics and a variety of application of these materials have been possible in different technological areas. In some field, like environment and energy, the porous ceramic materials may have enormous beneficial applications from the social and economic perspective(Al-Naib, 2018).

2.5.2 Classification of Porous Ceramic Materials

Porous ceramics can be classified depending on the nature of porosity, size of the pore and the volume fraction of the porous ceramic materials (Gaydardzhiev et al., 2008). Porous ceramic, generally, divided into two main categories, such as, ceramic foam and honeycomb ceramics (Liu & Chen, 2014). Ceramic foam consists of hollow polyhedron pores which form a three-dimensional array, and the honeycomb ceramic consists of columnar pores which usually form a two-dimensional array.

Ceramic foam is further divided into two classes: open cell, reticulated ceramic foam and closed cell, bubble like ceramic foam. The open cell ceramic foam and the close cell ceramic foams can be distinguished by the presence of solid cell walls as in case of closed cell ceramic foam, the pore is parted by solid cell walls (Colombo, 2006). Apart from these two classes of ceramic foams, there are some other classes of ceramics called half open cell ceramic foams, open pores at both ends and closed pores at both ends.

Figure 2.5

Ceramic with (A) Honeycomb Structure and (B) Foam Structure

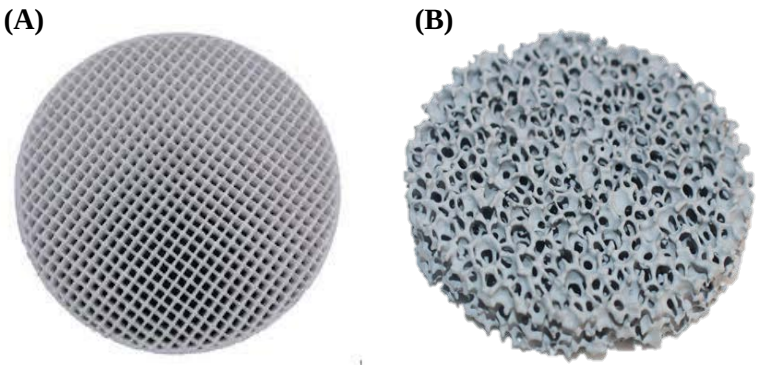

Based on the constituent materials, there are several types of porous ceramic materials: aluminosilicate, diatomite, silicate, silicon carbide, corundum, carbon and cordierites (Liu & Chen, 2014). Porosity of ceramic materials can be classified in different types, such as open porosity and closed porosity. Open porosity can be further divided into open dead-end pores and open pore channels. Depending on the accessibility of the materials to the surrounding media, the porous structure with different pore is shown by the following diagram (Rouquerol et al., 1994).

2.5.3 Characterization of Porous Ceramic Materials

Some general and most common characteristics (Liu & Chen, 2014) possessed by all types of porous ceramic materials are listed below:

a. Better chemical stability: Porous materials synthesized with appropriate constituent materials and preparation methodologies can be suitably used in the corrosive environment.
b. Good thermal stability: Porous materials made up suitable ceramic possessing heat-resistance property can be used as filter for burning gas at an elevated temperature or molten steel.
c. Good rigidity and specific strength: the size and shape of pores are constant and will not be changed under any stress, like liquid pressure, gas pressure etc.

d. Due to these characteristics porous ceramic materials can be a promising candidate in various technological fields, including environment protection, energy source, chemical engineering, electron industry, metallurgy etc.

2.5.4 Available Synthesis Methodologies for the Fabrication of Porous Ceramic Materials

Typically, there are a number of available methods for the preparation of porous nanomaterials. Some of the widely used methods are wet synthesis, sol-gel method, co-precipitation, impregnation and hydrothermal synthesis(Perera-Mercado et al., 2018). Among these methods, the most commonly used method is the hydrothermal synthesis which offers the formation of a nanomaterials with a variety of different shapes, including rods, spheres, wires, tubes, sheets etc.

Some other available synthesis methodologies are foam method, sponge method, injection molding leaching, emulsion templating, sintering of particles, gel casting etc. In order to produce complex ceramic materials, more sophisticated synthesis techniques are developed. One of such kind of method is solution-combustion method(Perera-Mercado et al., 2018).

2.6 Removal of Formaldehyde Using Alumina Polymer Nanocomposite

Alumina polymer composite are those materials that contains alumina with a polymer to show unique properties. When alumina nanoparticles are added to the polymer matrix it forms pores or void spaces in the interior structure of alumina polymer composite (Latief et al., 2019). The alumina polymer composites formed this way exhibits hardness, high tensile strength, stiffness, and lower density (Latief et al., 2019).

Amaro et al. reported the increase of mechanical strength of polymer to a great extent when filled with alumina nanoparticles. It also reported further enhancement of mechanical properties when the alumina nanoparticle filled polymer composites were treated with DDSA and MNA (Amaro et al., 2018).

Agarwal et al. reported the adsorption of formaldehyde using activate alumina (Agarwal & Dave, 2006). According to the study, when alumina is treated with suitable nucleophile, it exhibited enhanced formaldehyde adsorption. Activated alumina

adsorbents were treated with ammonia liquor like basic compound which offer basic moieties to adsorb formaldehyde.

2.7 Techniques to Test Formaldehyde Adsorption

Formaldehyde adsorption test were carried out in several different methods. For example, chamber method, cell method, desiccator method, gas analysis method, flask method, perforator method etc. (Salthammer et al., n.d.). however, the chamber method and cell method are time consuming and requires sophisticated instrumentation.

a. Perforator method (Hemmilä et al., 2018; Salem et al., 2011; Salthammer et al., n.d.): In this method, samples were boiled in toluene for 2 hours under reflux to extract formaldehyde from the samples. Then the formaldehyde was experimented by perforation in water. The amount of formaldehyde was investigated through photometric method using acetylacetone (Hemmilä et al., 2018). The moisture content of the sample affects the perforator value to a great extent. This method requires simple instrumentation and short analyzing time (3 hours) (Salthammer et al., n.d.).

b. Flask method (Salthammer et al., n.d.): Roffael et al. first developed this method (Salthammer et al., n.d.). In this method, sample specimen was placed in a closed bottle made of polyethylene. Then the sample piece was placed in distilled water overnight at a specified temperature. The water molecules absorbed the released formaldehyde which can be determined through photometric method.
    a. This method has some limitations, such as it allows the testing of small amount of sample and impractical open edge to surface ratio of the test specimen (Salthammer et al., n.d.). Despite the limitations, this method is used in various applications.

c. Desiccator method (Depeursinge et al., 2010; Salthammer et al., n.d.): This method is very similar to the flask method. Sample with known surface area was kept in desiccator and placed over water for 24 hours at a persistent temperature. Adsorbed formaldehyde was then analyzed by acetylacetone

method (Salthammer et al., n.d.). Unlike flask method, desiccator method offers the analysis of large volume of sample.

Desiccator method was also used by Srisuda et al.(Srisuda & Virote, 2008) to elucidate the adsorption capacity of the adsorbents. In this method they estimated the adsorption capacity of the amine functionalized mesoporous silica.

Figure 2.6

Instrumentation for Formaldehyde Adsorption Test(Salthammer et al., n.d.)

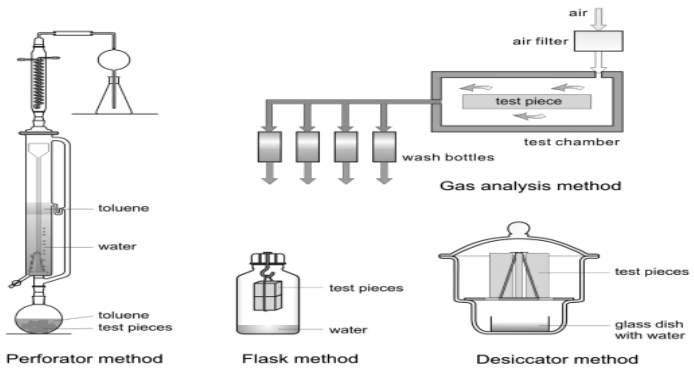

Gas analysis method (Salem et al., 2011; Salthammer et al., n.d.): This method is suitable to test the released formaldehyde at high temperature (60°C). In this method, the sample was taken in a test tube at a constant temperature (60°C). A stream of gas (1L per minute) was allowed to pass through the test tube. The formaldehyde emitted from the sample was absorbed by the gas which was then analyzed photometrically(Salem et al., 2011; Salthammer et al., n.d.).

2.8 Chapter Summary

Formaldehyde is a highly toxic volatile organic compound (VOC). In indoor atmosphere, it is usually emitted from the paint, furniture, floor materials etc. Formaldehyde causes severe health hazards, such as breathing problem, nausea and burning sensation in throat, eye, and nose (Ewlad-Ahmed et al., 2012). According to American Cancer Society, exposure to high concentration of formaldehyde can also cause cancer in human and animals. Hence, it becomes essential to remove formaldehyde from the indoor atmosphere.

Several methods, such as adsorption, advanced oxidation and scrubbing have been employed to remove formaldehyde from the atmosphere. Among all of these technologies, adsorption is the most widely used method for the removal of formaldehyde. Different sorbent materials, such as activated carbon, mixed metal oxide, mesoporous silica nanoparticles, activated alumina etc., are used to adsorb formaldehyde using physical, chemical, or physicochemical method.

CHAPTER 3
METHODOLOGY

3.1 Materials and Chemicals

3.1.1 Chemicals

Two alumina powder with different particle size was used: a) nm-sized γ-Al_2O_3 (Aluminium oxide C, Degussa, Germany, mean particle size=15 nm, specific surface area=100 m^2/g), b) µm-sized γ-Al_2O_3. Phenoxyethanol (POE), 1,6-Hexanedioldiacrylate (an acrylate ester monomer), proprietary photoinitiator (Irgacure 819, Aldrich, Germany), an azo dye as photoabsorber (Tinuvin 479, BASF Schweiz AG, Switzerland) was used to prepare the light casted ceramic. Tetraethoxysilane (TEOS) was used as silica precursor, A cationic surfactant n-Dodecyltrimethyl-ammonium bromide (sigmaaldrich, Germany) was used to form pore or as template, 37% (w/w) formaldehyde solution was used as adsorbate for the adsorption testing.

3.1.2 Apparatus and Glassware

Kakuhunter Planetary Mixer and Degasser (Glen Mills Inc.) was used to prepare homogeneous ceramic mixture, and a 405 nm light source was used to prepare the light casted ceramic. All the synthesized samples were sintered using a muffle furnace (Modutemp, Australia).

3.2 Synthesis of Sorbent Materials

Sorbent Material was prepared in two different approach. In the first approach, ceramic substrate was prepared by light casting process and then coated with amine functionalized mesoporous silica. on the other hand, in the second approach, the commercial alumina ceramic powder was directly dipped into the colloidal amine functionalized silica solution to prepare the amine functionalized silica coated alumina ceramic.

3.2.1 Synthesis of Amine Functionalized Mesoporous Silica Particles

Amine functionalized mesoporous silica was synthesized by sol- gel technique. Ethanol, water and ammonia were mixed together at a ratio of 20, 1200, and 10.4

respectively, to prepare the silica sol. Then CTAB (at a molar ratio of 0.3) was added to the solution and stirred the mixture for 15 minutes. After that, TEOS and APTES were added drop by drop to the mixture under the continuous stirring and continued for 2 hours at 60°C. The starting of the reaction was identified by the opacity of the mixture. After the completion of the reaction white powder was precipitated out and the mixture was then filtered and washed with deionized water. The particles were dried overnight and then placed at the furnace for calcination at 5°C/ mins to 550°C with holding time of 2 hours. The molar ratio of TEOS:EtOH:$NH_3 \cdot H_2O$:CTAB was fixed at 1:20:10.4:0.3. The molar ratio of H_2O was varied at three different composition (1200, 600 and 45.5) to get the desired morphology and the molar ratio of TEOS:APTES was varied at three different composition 99:1, 95:5, and 80:20 to achieve the optimum amine functionalization. Table 3.1 and Table 3.2 represents the synthesized samples with different designations according to their composition.

Table 3.1

Mesoporous Silica with Different H_2O/TEOS Composition Ratio

Sample ID	Composition ratio
MPS1	H_2O/TEOS = 1200
MPS2	H_2O/TEOS = 600
MPS3	H_2O/TEOS = 45.5

Table 3.2

Amine Functionalized Mesoporous Silica with Different TEOS/APTES Composition Ratio

Sample ID	Composition ratio
AMPS1	TEOS/APTES = 99/1
AMPS2	TEOS/APTES = 95/5
AMPS3	TEOS/APTES = 80/20

Figure 3.1

Synthesis of Mesoporous Silica Particles

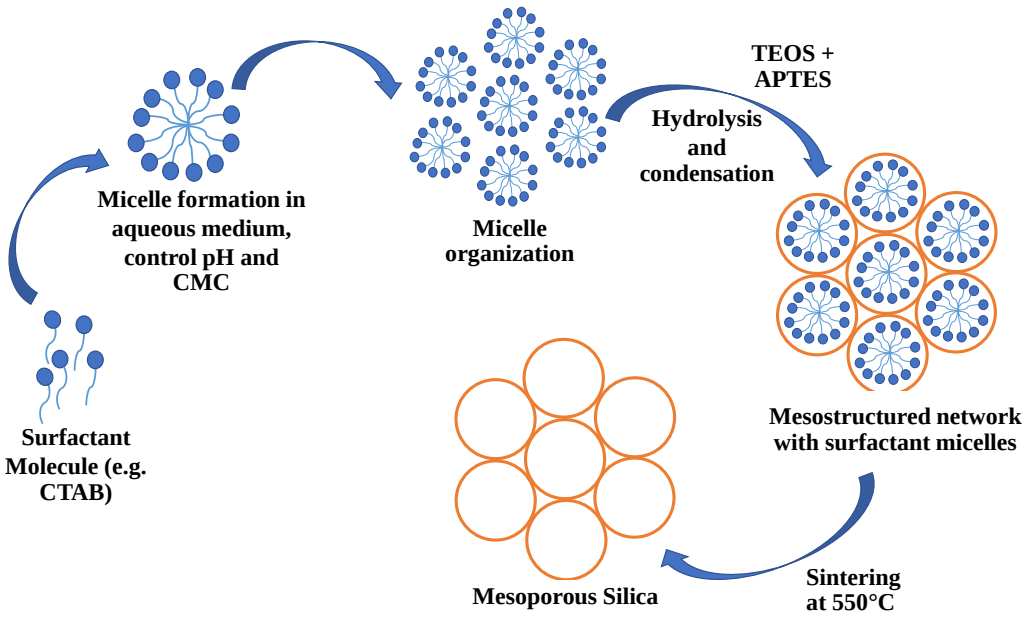

Figure 3.2

(A) Prepared Mesoporous Silica and (B) Amine Functionalized Mesoporous Silica

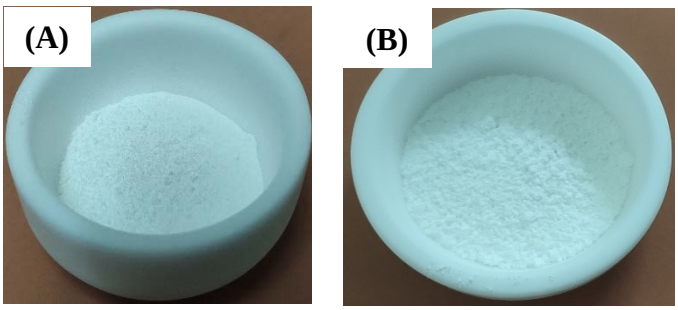

3.2.2 Synthesis of Ceramic Substrate

The ceramic substrate before sintering, also known as green ceramic substrate, is an alumina ceramic. To prepare the green ceramic body, at first, 30 wt% alumina particles was dispersed in 40 wt% phenoxyethanol (POE, Sigma Aldrich, Italy) by mixing in planetary mixer for 1 minute. Two types of alumina particle (µm- and nm-sized) was used to prepare alumina ceramic. The wight ratio between µm- and nm-sized alumina was optimized to prepare the ceramic with desired porosity. The mixture was then

allowed to stand for 30 minutes to ensure the complete dispersion of alumina particles in POE. After 30 minutes, 30 wt% 1,6-Hexanedioldiacrylate (an acrylate ester monomer), 0.2 wt% Irgacure 819 (a proprietary photoinitiator), and 0.06 wt% Tinuvin 479 (an azo dye as photoabsorber) were added to the mixture followed by mixing in a Kakuhunter Planetary Mixer and Degasser (Glen Mills Inc.) at 2000 rpm for 1 min to get a homogeneous mixture. The mixture will be exposed under a UV light source with a wavelength of 405 nm for 20 mins to get the complex green alumina ceramic. Then, the green ceramic will be sintered or calcinated in air in the muffle furnace at the 1400°C. The processing cycle of sintering in the air consists of two steps; the first step is debinding and the second step is firing at high temperature. In the debinding step the heating is carried out at 1°C/min rate to 700°C with a holding time of 1h to decompose the polymer network and in the second step the temperature is increased to 1400°C at a heating rate of 5°C/min with holding time of 1 h for the development of the ceramic structure.

Figure 3.3

Synthesis of Ceramic Substrate

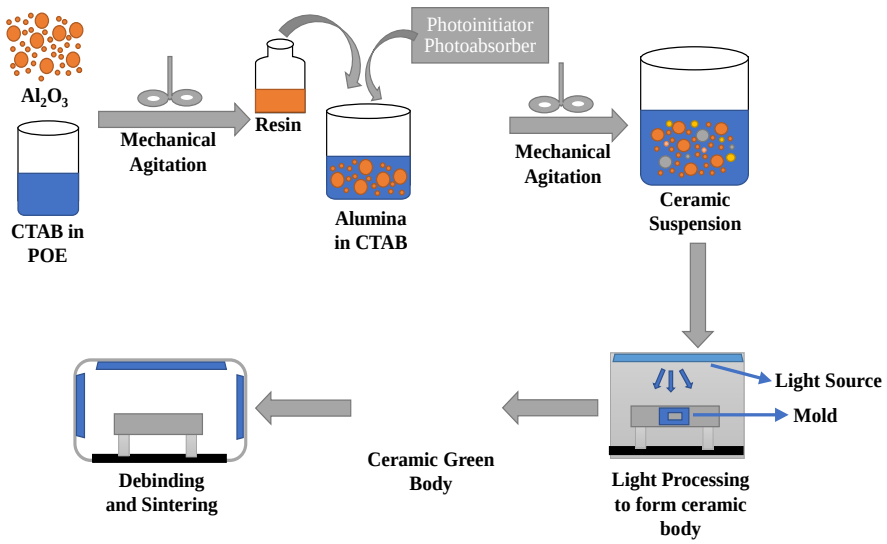

Figure 3.4

Ceramic Substrate (A) Before Sintering and (B) After Sintering

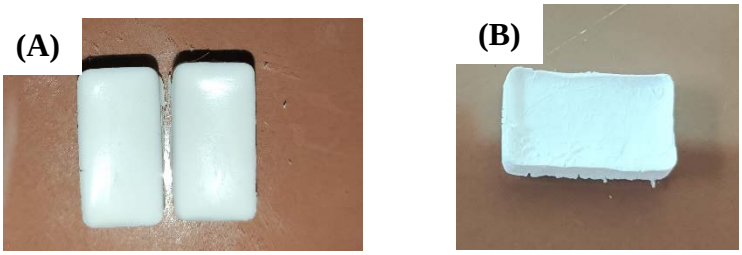

3.3 Coating of the Porous Ceramic Substrate with Mesoporous Silica Particles

Dip Coating process was carried out to coat the ceramic substrate with amine functionalized mesoporous silica particles. The coating process was carried out in two different approach. In the first approach, the light casted ceramic substrate was dipped into the amine functionalized mesoporous silica solution. The dipping time was varied as 1 min, 3 mins, and 5 mins and the dipping cycle was varied as 1 cycle, 2 cycles, 3 cycles optimized to get the suitable coating layer.

On the other hand, in the second approach, commercially available alumina powder was added to the amine functionalized silica solution to get the coated alumina particles. At first 0.5g of alumina powder was dipped into the amine functionalized mesoporous silica solution and allowed to stand overnight. Then the coated ceramic particles were filtered out of the solution followed by washing (3 times) with deionized water.

The sample obtained in both the approach was then sintered in the same procedure described in section *3.2.1*.

Figure 3.5

Fabrication of Mesoporous Silica Coated Adsorbent (A) approach-1 (Coating of Ceramic Substrate with Functionalized Silica Solution), and (B) Approach-2 (Coating of Alumina Ceramic Powder with Functionalized Silica Solution

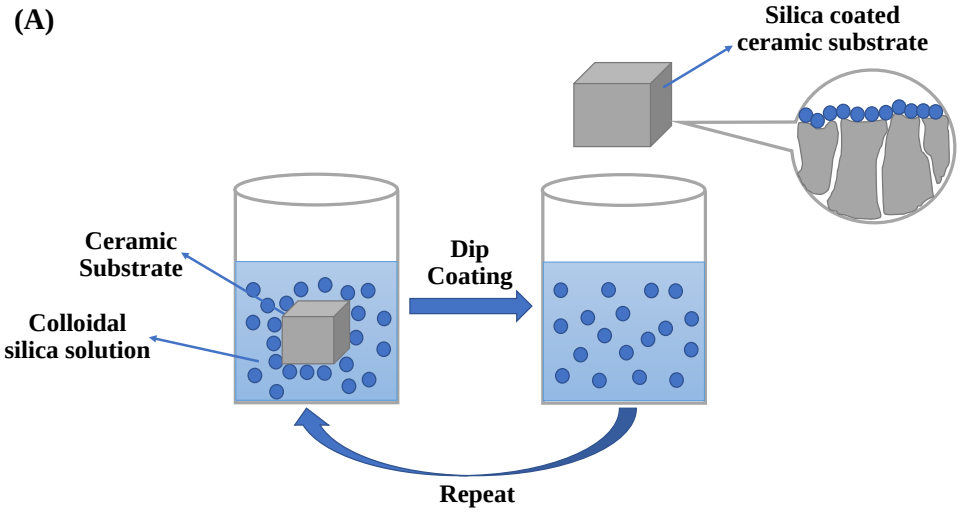

3.4 Characterization of Sorbent Materials

3.4.1 Morphological Characterization

Surface morphology and particle size were observed by Field Emission Scanning Electron Microscope (FESEM) using SU5000 microscope at National Science and Technology Development Agency (NSTDA). The acceleration voltage was 5 kV (0.1 kV step).

Energy Dispersive X-ray Spectroscopy (EDS) was used to observe the chemical constituents present in a sample. The selected area of the sample was scanned by FESEM with EDS. The accelerating voltage was 15 kV.

Fourier transform infrared spectroscopy (FT-IR) is a qualitative method to identify the functional groups of the synthesized chemical compounds. The samples were chemically analyzed by using Attenuated Total Reflection- Fourier Transform Infrared (ATR-FTIR) spectroscope. The spectra of the samples were analyzed from 4000 cm^{-1} to 400 cm^{-1}.

Micromeritics ASAP 2024 porosimeter was used to analyze the nitrogen adsorption isotherm to observe the structural property of the samples. The specific surface area (S_{BET}) and pore size was calculated from desorption curve by using Brunauer-Emmet-Teller (BET) method.

3.5 Formaldehyde Adsorption Testing

A HCHO testing chamber was developed which contains a hotplate, a pump, and a sensor. The chamber was sealed to ensure there was no leakage of formaldehyde molecule from the chamber. The hotplate was used to evaporate formaldehyde to ensure all the molecules of formaldehyde inside the chamber is in the gaseous form. The pump was used to circulate the air inside the chamber and a sensor was used to detect the change of formaldehyde value before and after exposure to the sample.

At first 52.7 µL of HCHO was placed on a hotplate inside the chamber at 40°C for 90 mins to convert the formaldehyde molecules from liquid form to gaseous form. Then the sample was exposed to the system. Gaseous HCHO molecules get adsorbed on the mesoporous silica sample and initial HCHO value starts to fall. Depending on the type of sample, the amount of adsorption was different.

Figure 3.6

Desiccator Method to Evaluate Formaldehyde Adsorption Efficiency of the Sorbent (A) Graphical Design (B) Actual Chamber

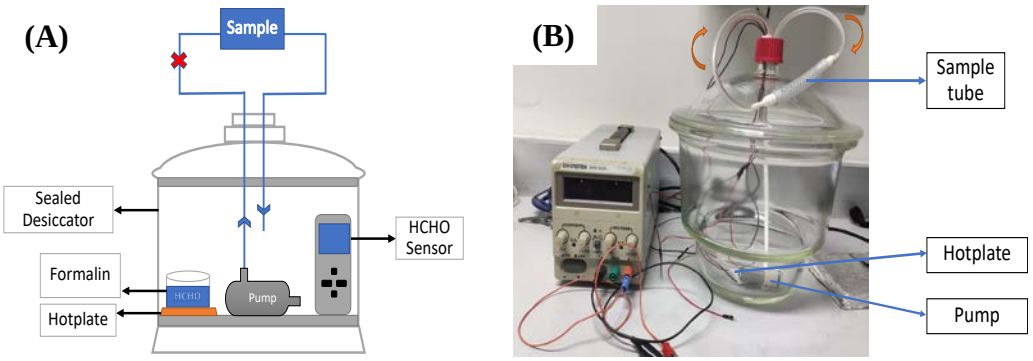

The mechanism behind the adsorption of formaldehyde by mesoporous silica followed the rection between amine group of amine functionalized silica and the carbonyl group of formaldehyde. The amine group reacted with the carbonyl group and forms imine bond which was responsible for the adsorption of formaldehyde on the silica surface. Adsorption of formaldehyde by amine functionalized mesoporous silica is shown by figure 3.7.

Figure 3.7

Adsorption of Formaldehyde on Amine Functionalized Mesoporous Silica Via Imine Group

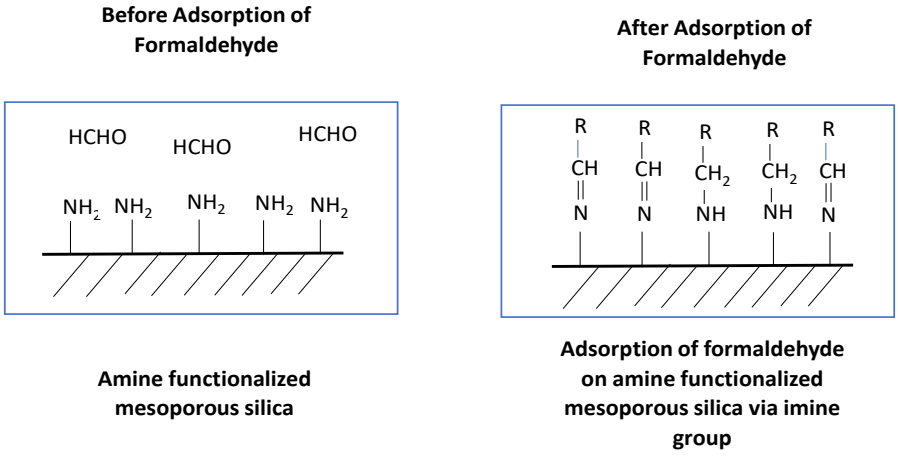

Figure 3.8

Mechanism of Reaction Between (A) Amine Group and Formaldehyde to Form Imine Group (B) Hydroxyl group and formaldehyde molecule

(A)

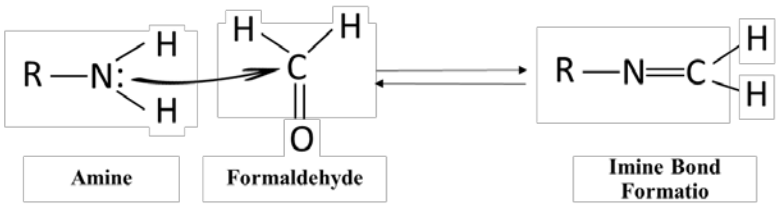

(B)

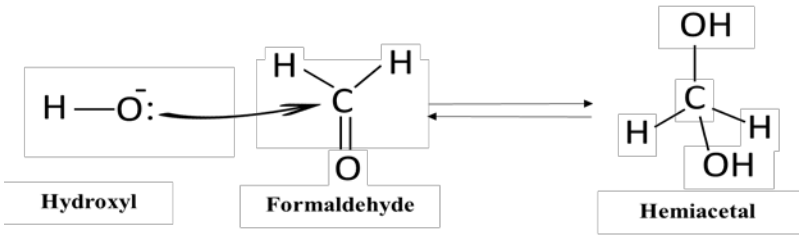

The amount of formaldehyde adsorbed on the sorbent was monitored by using a formaldehyde sensor. The sensor constantly monitored the concentration of formaldehyde gas. Therefore, the amount of formaldehyde adsorbed was determined by subtracting the formaldehyde concentration from the initial concentration which was used to determine the adsorption efficiency of the synthesized adsorbate.

The percent formaldehyde adsorption was estimated by using the following equation:

$$A_{FHD} = \frac{C_0 - C_t}{C_0} \times 100\% \quad \text{..... (i)}$$

Where, A_{FHD} is the amount of formaldehyde adsorbed at a certain time *t*, C_0 and C_t are the initial concentration of formaldehyde and concentration of formaldehyde at time *t*, respectively.

The adsorption capacity of the synthesized absorbate was determine by the following equation:

$$q_e = \frac{(C_0 - C_t)}{W} \times V \quad \text{.....(ii)}$$

Where, q_e is the adsorption capacity of the adsorbate, W is the mass of adsorbate and V is the volume of the chamber.

The adsorption data were determined at four different concentrations including 3 ppm, 6 ppm, 9 ppm, and 12 ppm and fitted to the Langmuir adsorption isotherm to determine the equilibrium adsorption characteristics. The linear formula of Langmuir isotherm can be shown as

$$\frac{C_e}{q_e} = \frac{1}{K_L q_{max}} + \frac{1}{q_{max}} C_e \ldots\ldots\ldots\ldots\ldots\ldots\ldots\ldots\ldots\ldots \text{(iii)}$$

Where, *Ce* is the equilibrium concentration of adsorbate (ppmv), q_e is the concentration of gas adsorbed on the sorbent (mg/g), K_L is the adsorption equilibrium constant in 1/mg and q_{max} is the maximum concentration of gas in mg/g adsorbed on the sorbent. The plot of C_e/q_e vs C_e gave a straight line with slope $1/q_{max}$ and intercept $1/K_L\, q_{max}$.

CHAPTER 4
RESULT AND DISCUSSION

Amine functionalized mesoporous silica coated ceramic materials were prepared for the adsorption of formaldehyde vapor. The sorbent materials were prepared in two different approaches. In the first approach, porous alumina substrate was first prepared using light casting method (λ = 405 nm) followed by sintering at 1400°C. Then the ceramic substrate was coated with amine functionalized mesoporous silica particles and sintered again at 550°C to prepare the sorbent material. On the other hand, in the second approach, the sorbent material was prepared by directly mixing the commercial ceramic alumina powder into a colloidal amine functionalized mesoporous silica nanoparticle dispersion followed by sintering at 550°C. The synthesized sorbent materials using the two approaches were tested for their adsorption performance against formaldehyde vapor in air by using a lab-based desiccator method and the adsorption data were fitted to the Langmuir isotherm to explain the mechanism of the adsorption process. This chapter summarizes the results obtained at various stages of the research and discuss them.

4.1 Characterization of Ceramic Substrate

4.1.1 Morphology Study of Alumina Ceramic Particles

Commercial alumina particles of two size ranges, one in µm-scale and one in nm-scale, were used to prepare the ceramic substrates. Figure 4.1 shows the FESEM micrographs of the as-received ceramic particles used in this study. From the SEM micrographs we observed that the nm-sized particles represented spherical shape due to the agglomeration of the particles, also known as granule. The particles can be redispersed by sonication. The µm-sized particles, on the other hand possessed an irregular anisotropic shape with sizes varied from about 100 nm to 4 µm. Both these sample were then used in the preparation of the sorbent materials as-received.

Figure 4.1

FESEM Micrographs (top view) of (A) nm-Sized and (B) µm-Sized Commercial Alumina Particles Used in This Study.

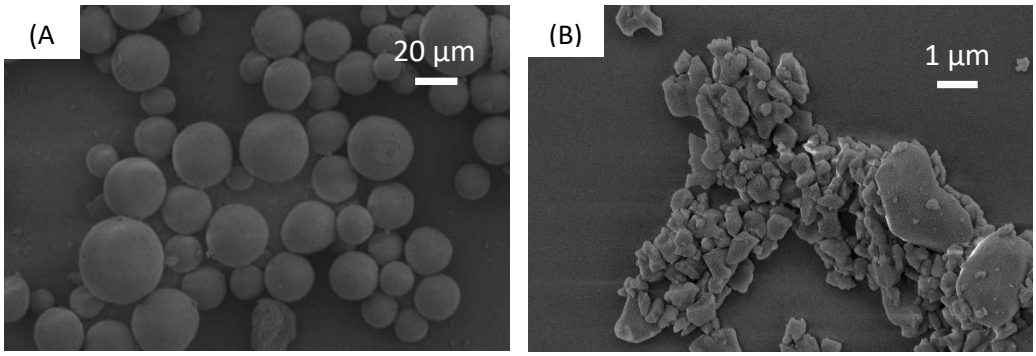

4.1.2 Morphology and Elemental Analysis of the Alumina Ceramic Substrates

Ceramic substrates were prepared by mixing the µm-sized and nm-sized alumina particles. Detailed preparation procedure of the alumina ceramic substrates is described in Chapter 3. FESEM micrographs showing the surface morphology of the alumina ceramic substrates prepared with the µm-sized and nm-sized alumina particles at two different mixing ratios are shown in Figure 4.2.

Figure 4.2

FESEM Micrographs of Alumina Ceramic Substrates (top-view) Prepared with (A) 100% µm-Sized Alumina Particles and (B) with 75% µm-Sized and 25% nm-Sized Alumina Particles.

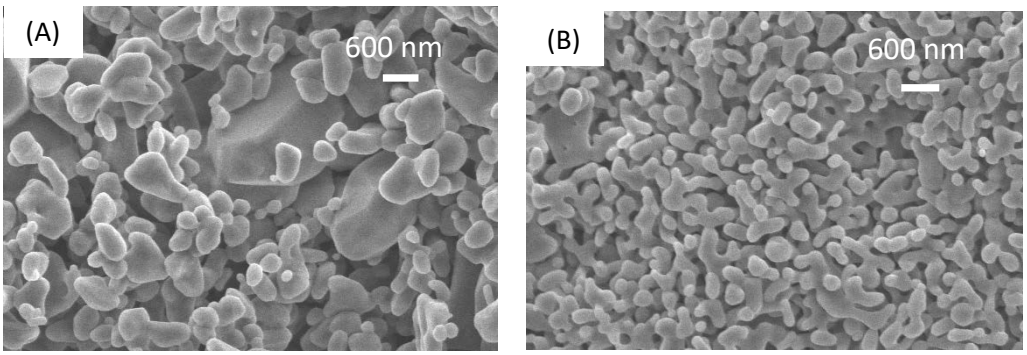

From the SEM images, it can be seen that the ceramic with 100% alumina particles possesses a rough surface while the ceramic with 75% µm-sized Alumina possesses

comparatively smoother surface. Due to the mixing of 25% nm-alumina the morphology of the ceramic changed significantly. The porosity and particle size of both the ceramic composition was found almost similar. Although the morphologically of the ceramic substrate with 25% nm- and 75% µm- sized alumina particles show more uniform surface and pore sizes, however, the ceramic substrates made up with this composition showed less stability during sintering and later coating with silica solution. Thus, the ceramic substrate prepared with 100% µm-sized alumina particles was chosen for the remaining experiments.

EDS analysis of a selected part of the ceramic substrate is shown in Figure 4.3 and the composition ratio of the elements are shown in Table 4.1. EDS analysis showed presence of Al and O in the substrate as major element with weight ratio 34.9% and 61.6%, respectively. This is close to the chemical formula of alumina, Al_2O_3, confirming its presence. A small amount of C (3.5 wt.%) was also found in the substrate which might be due to contamination during the sintering process ((Rešković, Brlić, Jakovljević, & Jandrlić, 2017).

Figure 4.3

EDS Spectrum of Ceramic Substrate Prepared with 100% µm-Sized Alumina Particles

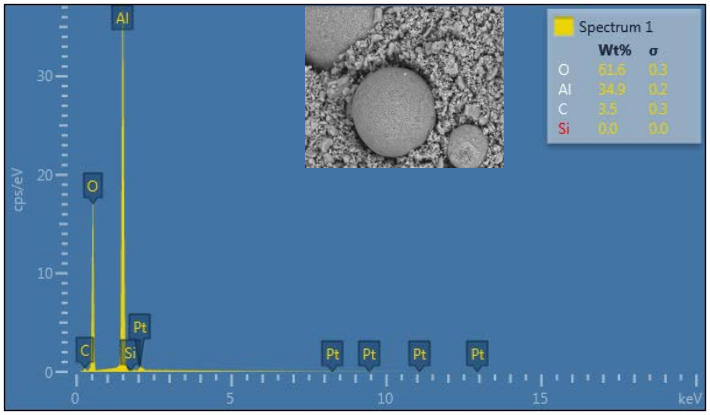

Table 4.1

Proportional Composition of the Elements Presents in The Ceramic Substrate Prepared With 100% µm-Sized Alumina Particles

Elements	Composition (wt%)
Oxygen (O)	61.6
Aluminum (Al)	34.9
Carbon (C)	3.5
Silicon (Si)	0

4.2 Characterization of Mesoporous Silica

4.2.1 Morphology and Particle Size Distribution of Mesoporous Silica by FESEM

Mesoporous silica particles were synthesized by sol-gel technique where the morphology and size distribution were varied by changing the amount of water content. The morphology of the particle depends on the concentration of water as the micelle formation mechanism and CTAB orientation depends on the formulation of precursors. Dilution of the solution influences the configuration of micelle which encapsulates the silica particles and determines the particle growth and shape. Figure 4.4 shows FESEM image of the mesoporous silica particles with variety of size and shape.

Figure 4.4

FESEM Micrographs of (A-1) MPS1, (B-1) MPS2 and (C-1) MPS3 Mesoporous Silica Particles and Their Corresponding Size Distribution Shown in (A-2), (B-2) and (C-2), Respectively.

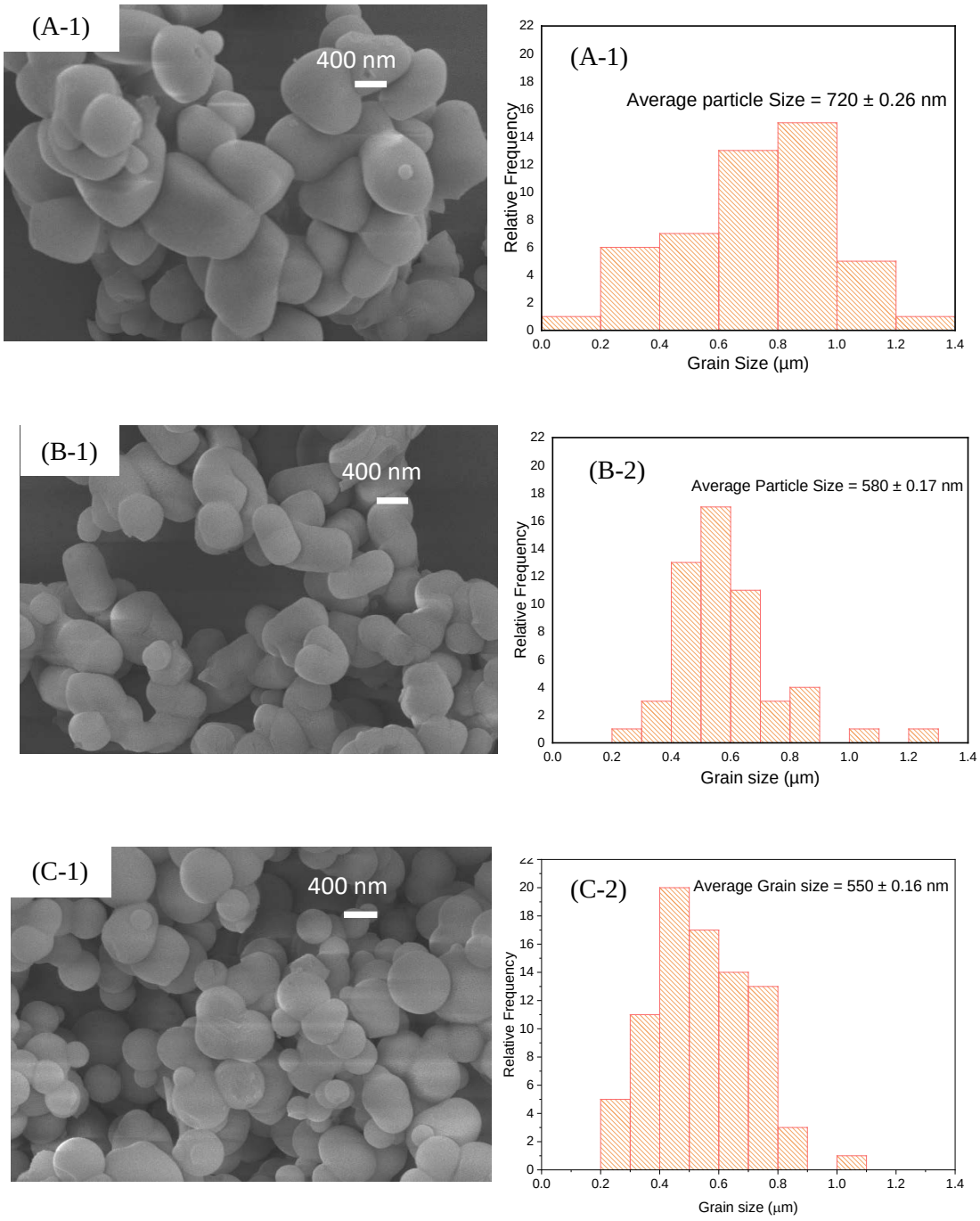

From Figure 4.4, we can see that the morphology of silica particles changes from rod shape to spherical shape as the amount of water in the precursor solution decreases. The mesoporous silica particles with molar ratio of H_2O/TEOS = 45 showed spherical shaped particles having average diameter of 550 nm whereas the particles with molar ratio of H_2O/TEOS = 600 and 1200 showed long range and short-range rod-shaped morphology having average particle size of 580 nm and 720 nm, respectively.

The histograms of particle size distribution of the mesoporous silica particle are shown in Figure 4.4 (A-2, B-2, and C-2). In general, all three compositions yielded particles in the range of 200 nm to 1.4 μm. However, from the histograms it can be seen that the mesoporous silica particles with H_2O/TEOS = 1200 exhibited a broader size distribution, while the particles with H_2O/TEOS = 600 and H_2O/TEOS = 45 showed comparatively narrower size distribution. The observations of FESEM analysis for the samples with different H_2O/TEOS composition is summarized in Table 4.2.

Table 4.2

Geometry and Average Particle Size of MPS1, MPS2 and MPS3 Mesoporous Silica Particles

Sample	Geometry	Average Particle Size (nm)
MPS1 (H_2O/TEOS = 1200)	Short rod	720 ± 0.26
MPS2 (H_2O/TEOS = 600)	Long rod	580 ± 0.17
MPS3 (H_2O/TEOS = 45)	Spherical	550 ± 0.16

4.2.2 Investigation of the Specific Surface Area and Porosity of the Mesoporous Silica Particles by BET and BJH Technique

The specific surface area, pore volume and pore size of the as-prepared mesoporous silica particles were analyzed by N_2 adsorption-desorption measurements using BET and BJH technique. For this experiment, we have chosen the MPS3 silica particles since they have shown smallest uniform spherical shape and narrow size distribution. Adsorption isotherm of MPS3 silica particles and their pore size distribution are shown in Figure 4.5.

Figure 4.5

(A) Adsorption Isotherm and (B) Pore Size Distribution of the MPS3 Mesoporous Silica Particle.

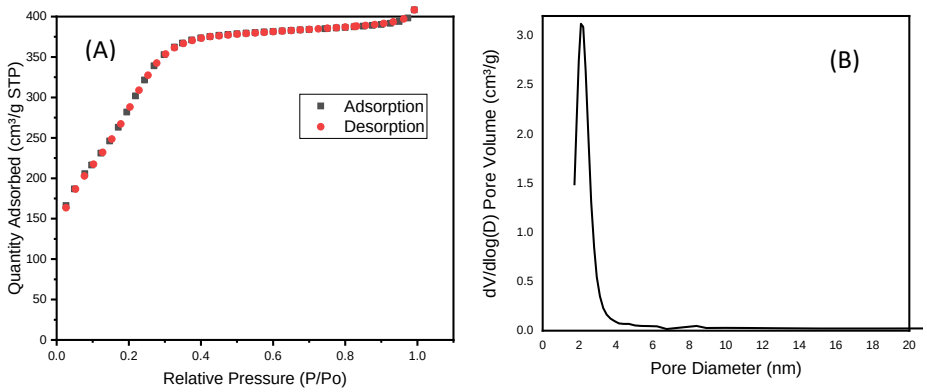

The above isotherm represents a type-IV adsorption isotherm, which is a characteristic isotherm of mesoporous materials. From the isotherms, the specific surface area (S_{BET}) of the mesoporous silica particle was estimated as 989 m^2/g, and the pore diameter was obtained as 2.4 nm indicating that the particles are mesoporous in nature with a pore volume of 0.6 cm^3/g. The result is comparable to the previous studies where it has been found that the similar precursor composition yielded particles with pore diameter of 2.7 nm and pore volume of 0.5 cm^3/g (Vazquez, Gonzalez, Ferrari, & Castro, 2017). BET results of the silica nanoparticles evidence the presence of mesoporous structure in the silica particles.

4.2.3 Analysis of the Functional Groups by FT-IR

FTIR was used to identify the functional groups present at the surface of the mesoporous silica particles. The FTIR spectrum of the MPS3 mesoporous silica is shown in Figure 4.6.

Figure 4.6

FTIR Spectrum of MPS3 Mesoporous Silica Particle

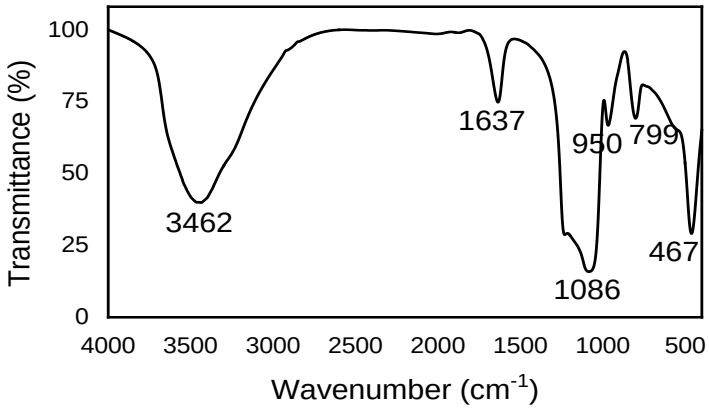

Silica contains silanol group (≡Si–OH) on the surface, thus, the broad band from 3700 to 2600 cm^{-1} observed in Figure 4.6 was attributed to the O-H bond stretching vibration. A strong band was observed at 1086 cm^{-1} which is due to the siloxane group (-Si-O-Si-); also showing a band from to 625 to 450 cm^{-1}. A small band at around 950 cm^{-1} was observed due to the stretching vibration of the silanol group (Si-O). Deformational vibration of water molecule was observed at around 1650 to 1600 cm^{-1} (Srisuda & Virote, 2008), indicating possibility of presence of some trapped water molecules in the mesoporous silica particles.

4.3 Characterization of Amine Functionalized Mesoporous Silica Particles

4.3.1 Morphology and Particle Size Distribution of Amine Functionalized Mesoporous Silica Particles

Amine functionalized mesoporous silica particles were synthesized with three different TEOS and APTES ratio. The FESEM image of three types of amine functionalized mesoporous silica is shown in Figure 4.7. FESEM image of mesoporous silica with composition H_2O/TEOS = 45 yielded spherical shaped particles with diameter 550 nm. Thus, this composition was chosen to prepare amine functionalized mesoporous silica particles.

Figure 4.7

FESEM Image (Top View) of Amine Functionalized Mesoporous Silica Particles (A) TEOS: APTES = 99:1, (B) TEOS: APTES = 95:5, and (C) TEOS: APTES = 80:20

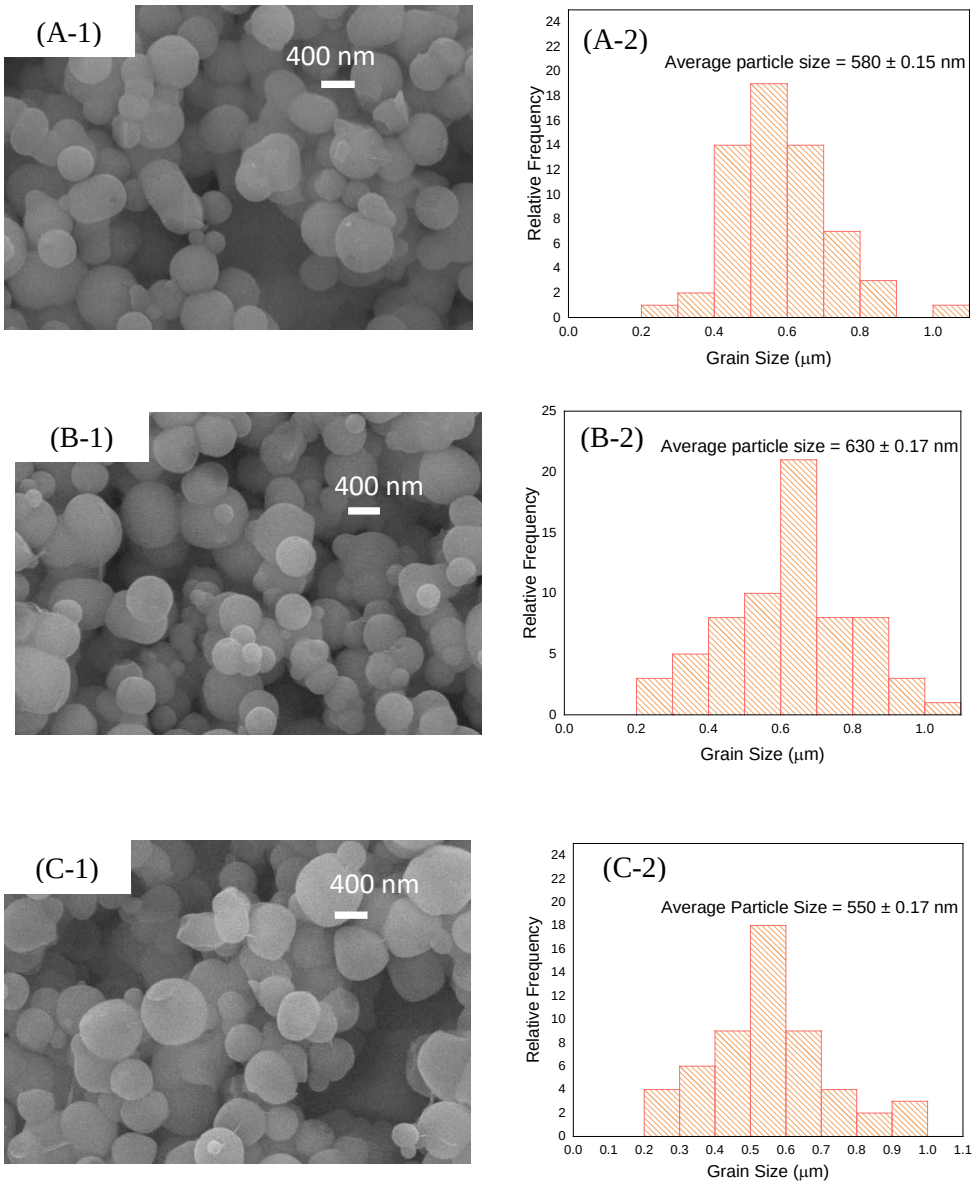

FESEM images shows that all the three of the TEOS/APTES compositions yielded spherical shaped particles. The average particle size varies from 550 to 630 nm. The morphology and particle size of the amine functionalized particle is summarized in table 4.3.

From the histograms it can be seen that all three of the compositions showed similar size distribution. Overall, it was found that the size of the particles varies from 200 nm to 1 µm and the majority of the particles reside in 400 to 800 nm range. From the above observation, it can be said that the average particle size varies slightly for all three of the compositions and the particle morphology is also similar, which indicates that the functionalization of silica particle with amine group does not have significant impact on the particle size and morphology.

Table 4.3

Morphology and Average Particle Size of AMPS1, AMPS2 and AMPS3

Sample	Morphology	Diameter (nm)
AMPS1 (TEOS/APTES = 99:1)	Spherical	580 ± 0.15
AMPS2 (TEOS/APTES = 95:5)	Spherical	630 ± 0.17
AMPS3 (TEOS/APTES = 80:20)	Spherical	550 ± 0.17

4.3.2 FTIR Investigation of Amine Modified Surface of Mesoporous Silica

The FTIR spectra of the amine functionalized mesoporous silica particles are shown in Figure 4.8, where amine functionalization was carried out at different amine concentrations.

Figure 4.8

FTIR Spectrum of the (A) AMPS1, (B) AMPS2, and (C) AMPS3 Silica Particles.

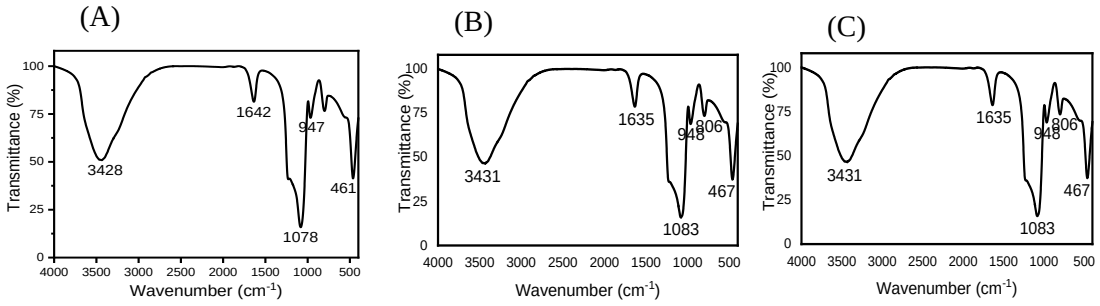

The stretching vibration of H-N bond in amine group (-NH_2) appears at 3450 to 3000 cm^{-1}. Note that this band has shifted almost 30 cm^{-1} towards higher wavenumbers compared to the silica particles without any amine functionalization (Figure 4.6). As observed in the Figure 4.8, the band at around 3431 cm^{-1} is due to the stretching vibration of amine group which overlapped with the band due to stretching vibration of hydroxyl (OH) groups. The bending vibration of amine group shows band between 1650 to 1580 cm^{-1}, thus the band at around 1642 cm^{-1} represents the bending vibration of amine group. All the data in the IR spectrum supports the presence of amine group in the structure.

4.3.3 Investigation of the Specific Surface Area and Porosity of Amine Functionalized Mesoporous Silica by BET and BJH Technique

N_2 adsorption desorption isotherm can be used to estimate the surface area (S_{BET}), pore size and pore volume. Figure 4.9 shows the adsorption isotherm and pore size distribution of amine functionalized silica particles.

Figure 4.9

(A) BET Adsorption Isotherm and (B) Pore Size Distribution of Amine Functionalized Silica Particles.

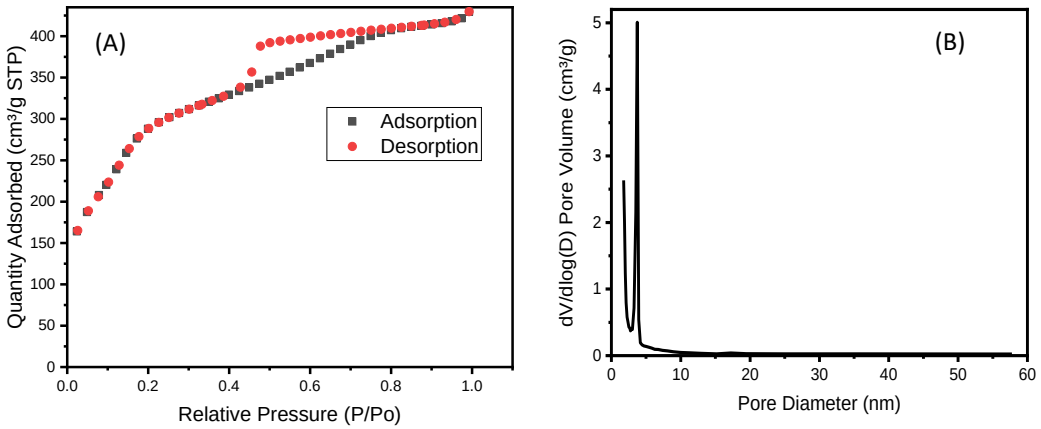

The above isotherm represents type-IV adsorption isotherm, which is a characteristic isotherm of mesoporous materials. From the isotherms, the specific surface area (S_{BET}) of the mesoporous silica particle was estimated as 949 m^2/g, which slightly decreased compared to the non-functionalized silica particles. The pore diameter was found

around 2.3 nm, and the pore volume is 0.6 cm^3/g similar to the silica particles without amine functionalization. BET results of the silica nanoparticles evidence the presence of mesoporous structure in the silica particles and indicated that the amine functionalization has negligible effect on the surface area and pore sizes of the silica particles.

4.3.4 EDS Investigation of Amine Groups on the Functionalized Mesoporous Silica

Energy Dispersive X-Ray Spectroscopy (EDS) was used to confirm the presence of amine groups on the mesoporous silica particles. The EDS image showing the N-mapping of the amine functionalized mesoporous silica particles is shown in Figure 4.10.

Figure 4.10

EDS Image of Amine Functionalized Mesoporous Silica Particles (A) AMPS1 (TEOS/APTES = 99:1), (B) AMPS2 (TEOS/APTES = 95:5), and AMPS3 (TEOS/APTES = 80:20) Showing The N-Mapping as Yellow Dots.

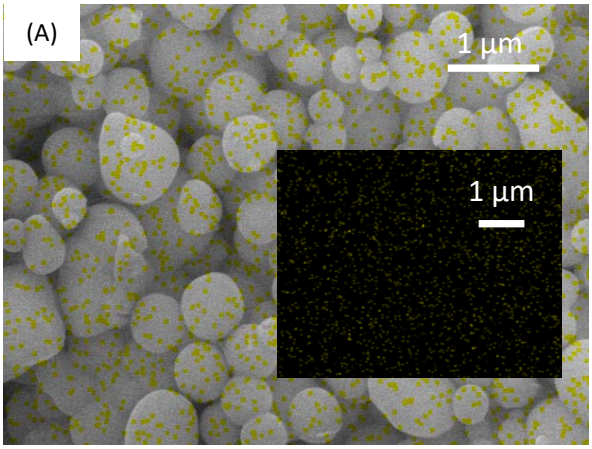

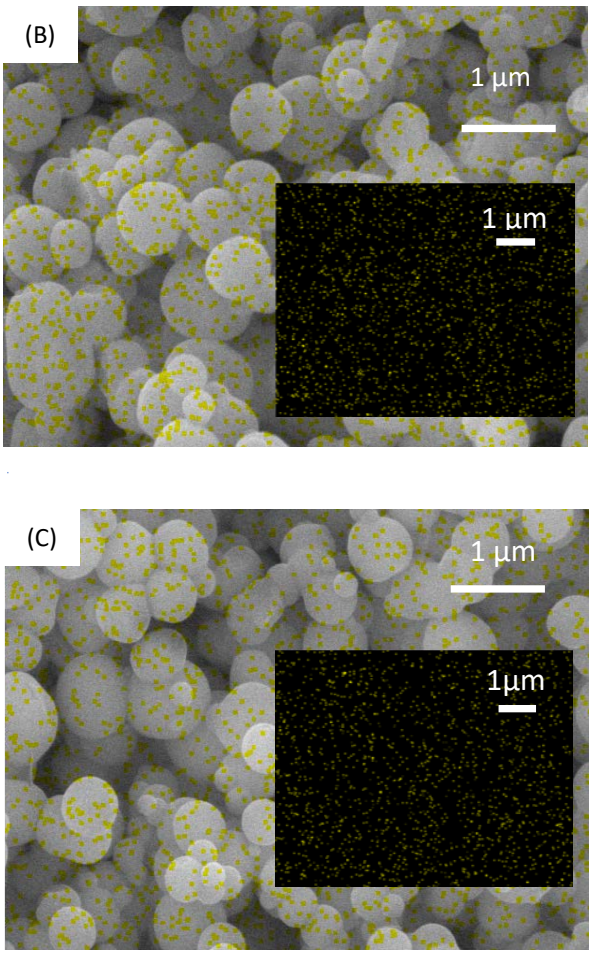

The yellow dots in the EDS image represents the nitrogen atom of the amine groups. From the images it can be confirmed that silica particles are bonded with the amine groups as N-atoms can be seen almost uniformly distributed all over the particle's surface. It can also be found that the density of nitrogen atom in AMPS3 (TEOS: APTES = 80:20) is higher than the other two compositions AMPS1 and AMPS2.

4.4 Comparison of Mesoporous Silica and Amine Functionalized Mesoporous Silica Particles

Mesoporous silica was prepared in three different compositions H_2O/TEOS = 1200, H_2O/TEOS = 600 and H_2O/TEOS = 45. Among all three of the compositions, H_2O/TEOS = 45 was chosen to prepare amine functionalized mesoporous silica due to the formation of spherical particle with high surface area. The particle morphology and

size of mesoporous silica and amine functionalized mesoporous silica obtained from FESEM image is shown in Table 4.4.

Table 4.4

Morphology and Particle Size of Mesoporous Silica and Amine Functionalized Mesoporous Silica by FESEM

Sample	Morphology	Diameter (nm)
Mesoporous Silica	Spherical	550 ± 0.16
Amine Functionalized Mesoporous Silica	Spherical	550 ± 0.17– 630 ± 0.17

FESEM images reveals that both mesoporous silica and the amine functionalized mesoporous silica are of spherical shape. The particle diameter of mesoporous silica was around 550 nm while that of amine functionalized mesoporous silica varies between 550 nm to 630 nm depending on the different composition of TEOS/APTES. Overall, both geometry and particle size of unfunctionalized and functionalized particles are same. Thus, we can say that the functionalization of mesoporous silica with amine group does not change the surface morphology and particle size.

FTIR spectrum was used to identify the characteristic functional group of the compounds. The FTIR spectrum presented indicates the presence of amine groups in the functionalized mesoporous silica sample. This was further confirmed using Energy Dispersive X-Ray Spectroscopy (EDS) with N-atom mapping showing the presence of amine groups in the mesoporous silica structure. The EDS spectrum of amine functionalized mesoporous silica is shown in Figure 4.11.

Figure 4.11

EDS Spectrum of Amine Functionalized Mesoporous Silica

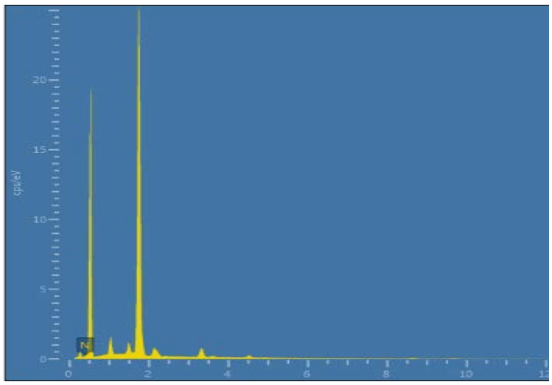

From the above elemental spectrum, it is evident that the amine functionalized mesoporous silica has nitrogen on its surface which is missing in the case of non-functionalized mesoporous silica.

The specific surface area and porosity of the mesoporous silica and amine functionalized mesoporous silica was studied from the N_2 adsorption desorption isotherm which is summarized in Table 4.5. Adsorption isotherm of both mesoporous silica and amine functionalized mesoporous silica exhibited type-IV adsorption isotherm which is the characteristic adsorption isotherm for mesoporous surface and showed similar pore size behavior.

Table 4.5

Comparative Specific Surface Area, Pore Size and Pore Volume of the Mesoporous Silica and Amine Functionalized Mesoporous Silica

Sample	Specific Surface Area, S_{BET} (m^2/g)	Pore Diameter (nm)	Pore Volume (cm^3/g)
Mesoporous Silica	989	2.4	0.6
Amine Functionalized mesoporous silica	949	2.3	0.6

The specific surface area (S_{BET}) of mesoporous silica was estimated as 989 m^2/g, while that of amine functionalized mesoporous silica was 949 m^2/g. The specific surface area of the mesoporous silica reduced slightly after functionalization which might be due to the crowding on silica surface by amine groups. The pore diameter and pore volume of amine functionalized mesoporous silica remains the same as the non-functionalized mesoporous silica particles. Therefore, we can reach to the conclusion that, the functionalization of mesoporous silica does not have high impact on the specific surface area and porosity of the particles.

4.5 Characterization of Amine Functionalized Mesoporous Silica Coated Ceramic Sorbent

The amine functionalized mesoporous silica coated ceramic sorbent was prepared in two different approach. In the first approach light casted ceramic was prepared and then dipped into the colloidal amine functionalized mesoporous silica solution to coat the ceramic. In the second approach, the alumina ceramic powder was directly dipped into the amine functionalized silica solution to coat the ceramic powder particles. The FESEM image of both the coated light casted ceramic and coated ceramic powder is shown in Figure 4.12

Figure 4.12

FESEM Images of (A) Cross-Section of Coated Light Casted Ceramic and (B) Coated Ceramic Powder

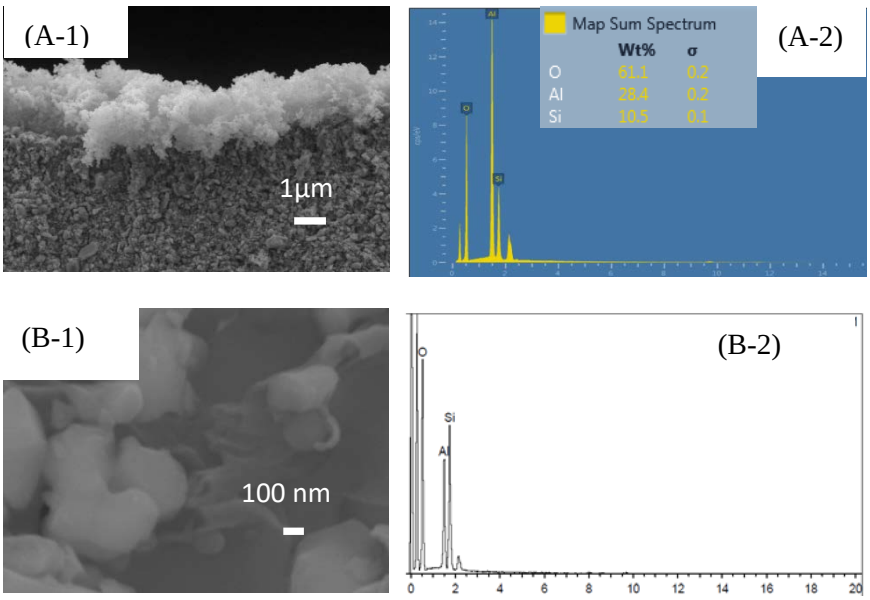

From the FESEM image of the coated light casted ceramic (A-1) and the EDS spectrum (A-2), it was found that the silica particles are present in the sample. However, FESEM image reveals that the size of silica particle is bigger than the pore channel of the light casted ceramic, hence, the silica particles were not entering into the channels of the ceramic structure; rather sitting on the ceramic surface. Therefore, the silica coated ceramic sorbent was prepared in another approach where the ceramic powder particles are coated with the amine functionalized silica particles.

The FESEM image of the coated alumina particles (B-1) did not show the silica particles clearly on alumina particles. However, the EDX spectrum (B-2) confirms the presence of silica in the sample, as indicated by the presence of a strong Si peak.

4.6 Determination of the Formaldehyde Adsorption performance of the Sorbents

The formaldehyde adsorption efficiency of the synthesized samples was tested by desiccator method. At first 68.9 µL of formaldehyde was placed on a hotplate at 40°C inside an 8.5 L desiccator and waited for 90 mins to reach the initial formaldehyde concentration inside the chamber at around 3 ppm. After 90 mins the 0.5g of each sample was exposed to formaldehyde gas and the adsorption efficiency the samples were recorded against time. Detailed experimental conditions and procedures are described in Chapter 3.

The formaldehyde adsorption performance of uncoated ceramic, mesoporous silica (MPS), amine functionalized mesoporous silica (AMPS), amine functionalized mesoporous silica coated light casted ceramic and amine functionalized mesoporous silica coated alumina powder was compared, which is shown in Figure 4.13.

Figure 4.13

Formaldehyde Decay Plot of Uncoated Ceramic, MPS powder, AMPS powder, AMPS Coated Light Casted Ceramic and AMPS Coated Alumina Powder as a Function of Time

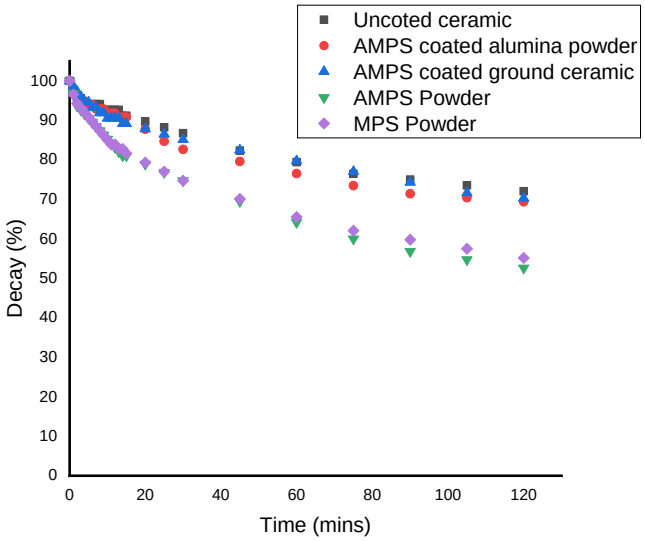

As observed in Figure 4.13, the adsorption performance of ceramic support samples is very less compared to the MPS and AMPS powder. As the silica particles are quite large compared to the channels and pores of the ceramics, thus the particles were sitting on the surface of ceramic samples. The amount of silica was, in turn, very low in the ceramic support samples. As a result, we could not see much impact of the sorbent material towards the formaldehyde adsorption. Therefore, we focused on the formaldehyde adsorption efficiency of functionalized and unfunctionalized mesoporous silica samples. Among all the samples, AMPS was showing better adsorption. Thus, we tested three different composition of AMPS to get the optimum composition ratio.

The formaldehyde adsorption efficiency of amine functionalized (AMPS1, AMPS2, and AMPS3) and unfunctionalized mesoporous silica (MPS) was tested and the data were recorded against time. The plot of adsorption efficiency of different powder sample is shown in Figure 4.14.

Figure 4.14

Formaldehyde Decay Plot of MPS, AMPS1, AMPS2, and AMPS3 as a Function of Time. Amount of Sorbent Material was Kept Constant at 0.5g.

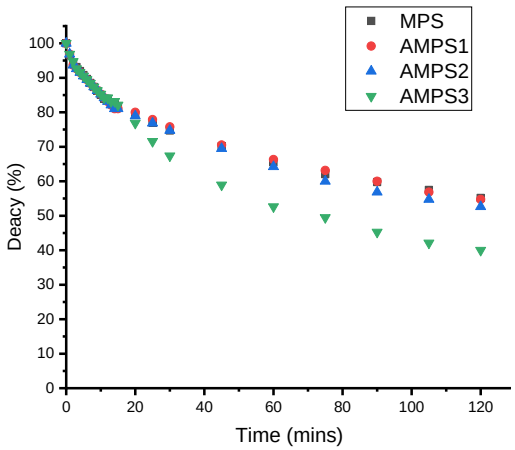

From the decay plot (Figure 4.14), we can see that the 0.5g of each sample is capable of adsorbing almost 40% of 3 ppm formaldehyde within 2 h. However, the AMPS3 showed better adsorption efficiency (60%) towards formaldehyde. The concentration of formaldehyde inside the chamber dropped down from 3 ppm to 1.2 ppm by AMPS3. The other functionalized and unfunctionalized mesoporous silica are showing almost same adsorption efficiency.

Plot of adsorbate concentration as a function of time of MPS, AMPS1, AMPS2 and AMPS3 can be plotted to estimate their adsorption profile which are presented in Figure 4.15.

Figure 4.15

(A) Plot of Formaldehyde Adsorbed on MPS, AMPS1, AMPS2 and AMPS3 (B) Enlarge View of First 15 Mins (C) Enlarge View of 20 to 60 Mins (D) Enlarge View of 60 Mins to 120 Mins

(A) (B) (C)

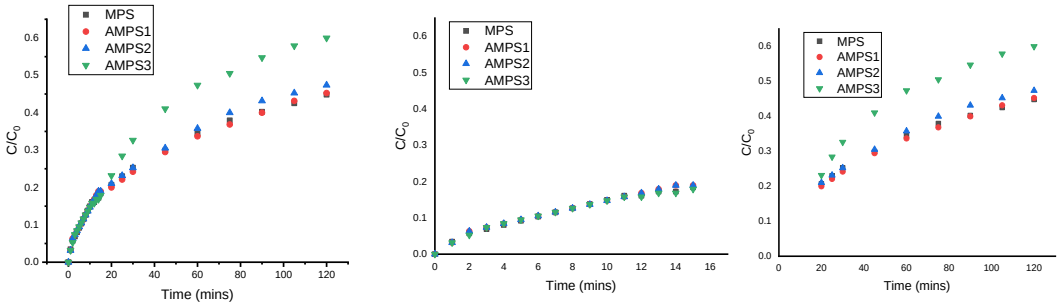

From the adsorption performance observed in Figure 4.15(A), it is evident that MPS, AMPS1 and AMPS2 exhibit comparable adsorption capacity. However, AMPS3 showed better adsorption performance. The adsorption performance of the samples at different time was split into three different segment and the adsorption performance of the samples were observer. Figure 4.15 (B) represented the adsorption performance of all the samples in the initial 15 mins. It can be seen from the Figure that the initial adsorption performance of all the sample was very similar as all the sample has enough active sites to adsorb the formaldehyde molecules. However, difference in adsorption performance was observed after 15 mins shown in Figure 4.15 (C) which is followed until 2h.

AMPS3 (with 20% APTES) started showing better adsorption performance than the other three samples. This might be due to the presence of highest number of amine groups on the adsorbent surface which interacted with the formaldehyde molecules resulting in adsorption; this is supported by the EDS results as well. The EDS images in Figure 4.10 confirmed the presence of highest amount of amine groups in AMPS3 (Figure 4.10C). As observed in EDS results, amine groups are functionalized on the surface of the samples which interacted with the formaldehyde molecules. Thus, the adsorption capacity of the samples depends on the available surface amine groups. In

addition to the amine groups, the adsorption happens on the pores of the adsorbents as well.

Adsorption performance was also observed for unfunctionalized mesoporous silica. Mesoporous silica has hydroxyl group (-OH) on the surface which can interact with the formaldehyde molecule resulting in adsorption. However, the adsorption capacity of amine functionalized mesoporous silica is better than the unfunctionalized silica. The higher adsorption capacity of amine functionalized sorbent might be attributed to the strong interaction of the amine group with formaldehyde molecule than hydroxyl group.

Both the amine (-NH_2) and hydroxyl (-OH) groups contain lone pair of electrons; through which they interact with the formaldehyde molecules(Meyer, Joiner, & Stoddart, 2007; Swain, Powell, Sheppard, & Morgan, 1979) as shown in Figure 4.16. However, the electron donation is easier for amine group than hydroxyl group as the electronegativity of the nitrogen (N) atom is lesser than the oxygen (O) atom(Pauling, 1932). Therefore, amine functionalized mesoporous silica showed better adsorption capacity than the unfunctionalized mesoporous silica.

Figure 4.16

Mechanism of Reaction Between (A) Amine and Formaldehyde and (B) Hydroxyl and Formaldehyde.

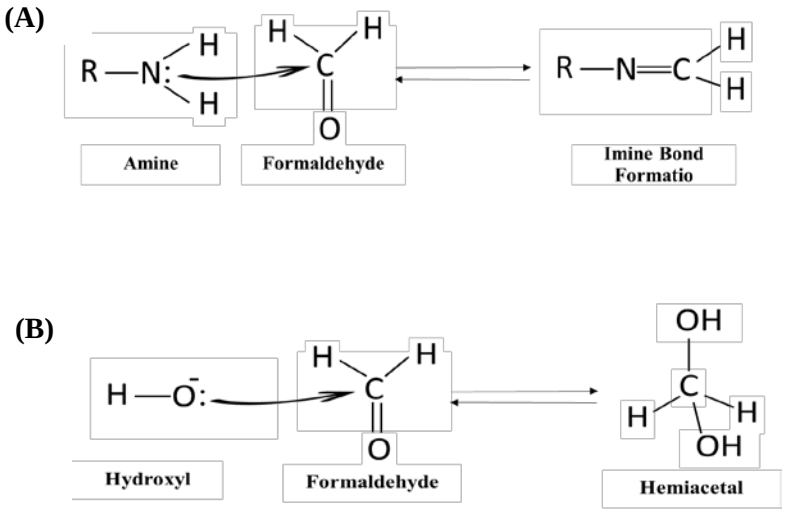

AMPS1 and AMPS2 was showing slightly better adsorption than MPS due to the presence of very less amount of amine group (1% amine group in AMPS1 and 5% amine group in AMPS2) in addition to the hydroxyl groups. The comparative adsorption efficiency of the samples at 2h can be shown by the Figure 4.17.

Figure 4.17

Comparative Adsorption Efficiency of MPS, AMPS1, AMPS2 and AMPS3 at 2h

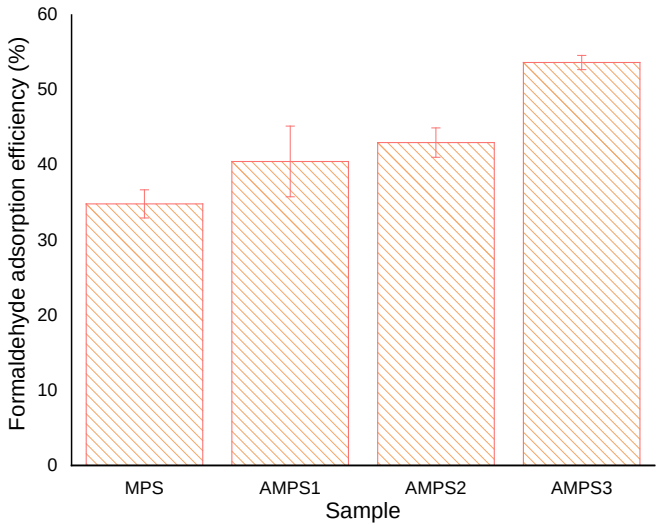

As observed in Figure 4.15 and Figure 4.17, AMPS3 was demonstrating better adsorption performance and capable of removing highest amount of formaldehyde, thus we chose this composition to further confirm the adsorption mechanism. Adsorption capacity of AMPS3 was measured at different equilibrium concentrations of formaldehyde and fitted to the Langmuir isotherm model to determine the adsorption characteristics at equilibrium condition. Plot of adsorption capacity of AMPS3 against time at different concentration of formaldehyde is shown in Figure 4.18.

Figure 4.18

Plot of Adsorption Capacity vs Time of AMPS3 at (A) 3 ppm, (B) 6 ppm, (C) 9 ppm, (D) 12 ppm and (F) Langmuir Isotherm of AMPS3

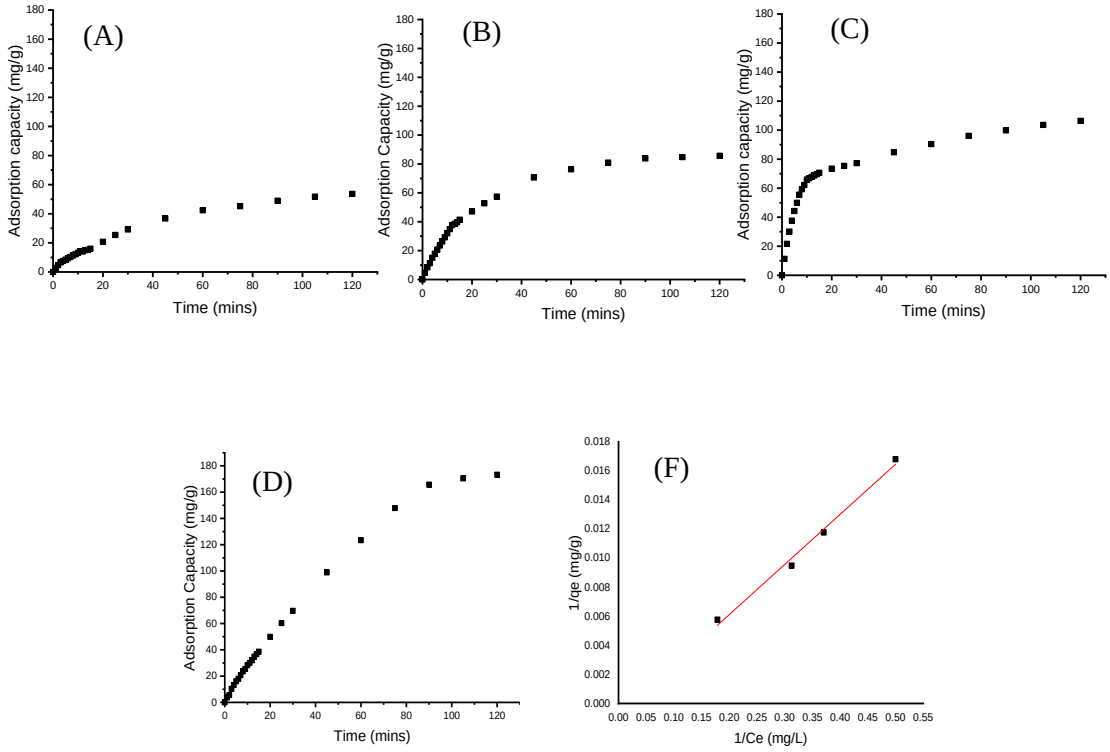

Four different concentrations, 3ppm, 6ppm, 9ppm and 12ppm of AMPS3 were used and the data were recoded for 2 hours. The obtained data were fitted to the Langmuir equation and the parameters of the isotherm are shown in table 4.6. Maximum adsorption capacity of the sample was determined from Langmuir adsorption isotherm which corresponds to the formation of complete monolayer on the adsorbent. The q_{max} value of AMPS3 was found as 1227 $\pm$ 51.1 mg/g and the K_L was found as 26 $\pm$ 0.006 $\times 10^{-3}$ per gram of sample.

The R^2 value indicated the data are well fit to Langmuir isotherm model. This indicates the adsorption of formaldehyde gas on the adsorbent surface occurring through the monolayer formation, which supports the adsorption of the gas through chemical interaction. The q_{max} represented the maximum adsorption capacity of the adsorbent and the K_L represented the adsorption equilibrium constant (1/mg).

Replicate data were recorded to make the Langmuir adsorption isotherm, the parameters of the isotherm of are shown in table 4.6

Table 4.6

Formaldehyde Adsorption Isotherm Parameters

Sample	q_{max} (mg/g)	K_L (1/mg)	R^2
AMPS3	1227 ± 51.1	$26 \pm 0.006 \times 10^{-3}$	0.9977

q_{max}: adsorption capacity (mg/g); K_L: adsorption equilibrium constant, K_L (l/mg)

Therefore, from the observed results it can be summarized that the adsorption capacity of the sample largely depended on the surface morphology and textural characteristics. The functionality played the major role towards the adsorption process. This was justified by the EDS and IR results. In addition, the specific surface area and pore diameter also showed significance in formaldehyde adsorption.

CHAPTER 5
CONCLUSION AND FUTURE RECOMMENDATION

5.1 Conclusions

Amine functionalized mesoporous silica was prepared in two different approach. In the first approach, the ceramic substrate was prepared and coated with silica particles. However, the size of the silica particles was bigger than the pore channel of the ceramic. Thus, the coated silica was only sitting on the surface of the ceramic substrate instead of entering into the channels of the substrate. To avoid the problem, the commercialized alumina was directly dipped into the silica solution and coated with the silica particles. Morphological, textural, and chemical properties of the synthesized samples were studied with different spectroscopic techniques. The adsorption performance and efficiency of the synthesized sorbent was studied with desiccator method and the data obtained were fitted to the Langmuir isotherm to elucidate the adsorption characteristic of the adsorbents.

The specific surface area and the pore diameter of the mesoporous silica and amine functionalized mesoporous silica are similar. This indicates the surface functionalization of silica with amine group does not have any significant impact on the morphological and textural property of the synthesized materials.

The adsorption of formaldehyde on the amine functionalized mesoporous silica occurs through the reaction between the formaldehyde molecule and the amine groups present on the adsorbent surface. In absence of amine group, the hydroxyl groups of silica participate in the reaction and forms bond with the formaldehyde molecules. However, the hydroxyl groups react slowly with the formaldehyde due to the higher electronegativity of the oxygen atom than nitrogen in amine. Thus, the unfunctionalized silica shows lower adsorption capacity than the amine functionalized silica.

Among all the synthesized samples, the AMPS3 adsorbed highest amount (60%) of formaldehyde. Therefore, the adsorption data of AMPS3 were fitted to the Langmuir isotherm model to elucidate the adsorption characteristics. Adsorption data were well fitted to the Langmuir isotherm in terms of R^2 value (0.99). The results obtained in the

current research was compared with the previous studies and shown in table 5.1 and table 5.2.

Table 5.1

Comparison of Structural Parameters of The Present Work with The Previous Works

Ref.	Precursor Solution	Specific Surface Area, (m^2/g)	Particle Size (nm)	Pore Diameter (nm)
Current Study	TEOS(TEOS:APTES= 80:20):EtOH: $NH_3 \cdot H_2O$:CTAB: H_2O = 1:20:10.4:0.3:45.5	949	550	2.3
(Srisuda & Virote, 2008)	TEOS:AEAP:CTAB: EtOH:H_2O = 0.85:0.15:0.22:5:80	141.40	-	159.8
	TEOS:AEEA:CTAB: EtOH:H_2O = 0.85:0.15:0.22:5:80	8.14	-	177.7

Table 5.2

Comparison of The Adsorption Characteristics of The Present Work with The Previous Works

	Current Study	Reference (Srisuda & Virote, 2008)	
Precursor	TEOS +APTES	TEOS + AEAP	TEOS + AEEA
Adsorption Capacity, q_{max} (mg/g)	1227 ± 51.1	1208	613.88
adsorption equilibrium constant, K_L (l/mg)	$26 \pm 0.006 \times 10^{-3}$	1.10×10^{-4}	3.45×10^{-4}
R^2	0.9977 ± 0.001	0.9603	0.9935

APTES: (3-Aminopropyl) triethoxysilane; AEAP: n-(2-amino-ethyl)-3-amino-propyltrimethoxysilane; AEEA: 3-(2-(2-amino-ehtylamino)ethylamino) propyltrimethoxysilane.

As observed in table 5.1 and 5.2, the specific surface area of the synthesized compound under current study using TEOS and APTES is 949 m^2/g, which is significantly high compared to the previous studies where instead of APTES, AEAP and AEEA were used. On the contrary, the pore diameter of our synthesized sorbent sample is also considerably smaller than the other works.

In the current study, the sample synthesized with highest amount of amine group showed highest adsorption capacity; one gram of the sample was adsorbing 1227 $\pm$ 51.1 mg/g of formaldehyde. However, in previous studies it has been seen that the adsorption capacity of the compound synthesized from AEAP was 1208 mg/g while the compound synthesized from AEEA adsorbed 613 mg/g formaldehyde. APTES, AEAP and AEEA contain one, two and three amine groups in their structure, respectively, which proves that large number of amie containing ligands do not necessarily offer high adsorption capacity. Therefore, from the observation we can say that amine groups are not solely responsible for the adsorption; morphological and structural features including the specific surface area and pore diameter are also responsible for the high adsorption capacity of the synthesized sample.

5.2 Future Recommendations

Further investigation in this field is highly required to prepare adsorbents with enhanced performance. Three different ratios of TEOS/APTES were tried under this work, which showed that higher amount of amine groups offer better adsorption capacity. Thus, the other TEOS/APTES ratios need to be tested in future to get the optimum amount of amine groups with highest efficiency. The particle size of the synthesized mesoporous silica was around 500 nm which need to be reduced to $\leq$50 nm by tuning the synthesizing condition and precursor composition ratio; so that the particle can enter into the pores and channel of the ceramic substrates. The ceramic substrate preparation methodology also needs to be modified in future to get more porous substrate with bigger pore diameter. Stability of the ceramic substrates also needs further investigation which was not considered in the current study.

REFERENCES

Agarwal, M., & Dave, M. (2006). Adsorption of Formaldehyde on Treated Activated Carbon and Activated Alumina. *Current World Environment, 1*(1), 53–59. https://doi.org/10.12944/cwe.6.1.06

Alam, M. A., & Al Riyami, K. (2018). Shear strengthening of reinforced concrete beam using natural fibre reinforced polymer laminates. *Construction and Building Materials*, *162*, 683–696. https://doi.org/10.1016/j.conbuildmat.2017.12.011

Al-Naib, U. M. B. (2018). Introductory Chapter: A Brief Introduction to Porous Ceramic. *Recent Advances in Porous Ceramics*, 1–10. https://doi.org/10.5772/intechopen.74747

Amaro, A. M., Pinto, D. G., Bernardo, L., Lopes, S., Rodrigues, J., & Louro, C. S. (2018). Mechanical Properties of Alumina Nanofilled Polymeric Composites Cured with DDSA and MNA. *Fibers and Polymers*, *19*(2), 460–470. https://doi.org/10.1007/s12221-018-7664-7

Amgoune, A., Krumova, M., & Mecking, S. (2008). Nanoparticle-supported molecular polymerization catalysts. *Macromolecules*, *41*(22), 8388–8396. https://doi.org/10.1021/ma801995g

Báez, A., Padilla, H., García, R., Torres, M. D. C., Rosas, I., & Belmont, R. (2003). Carbonyl levels in indoor and outdoor air in Mexico City and Xalapa, Mexico. *Science of the Total Environment*, *302*(1–3), 211–226. https://doi.org/10.1016/S0048-9697(02)00344-3

Bhatia, S., & Bhatia, S. (2016). Nanotechnology and Its Drug Delivery Applications. In *Natural Polymer Drug Delivery Systems* (pp. 1–32). Springer International Publishing. https://doi.org/10.1007/978-3-319-41129-3_1

Branković, M. D., Zarubica, A. R., Anđelković, T. D., & Anđelković, D. H. (2017). Mesoporous silica (MCM-41): Synthesis/modification, characterization and removal of selected organic micro-pollutants from water. Advanced Technologies, 6(1), 50-57.

Brigante, M., & Avena, M. (2014). Synthesis, characterization and application of a hexagonal mesoporous silica for pesticide removal from aqueous solution. Microporous and mesoporous materials, 191, 1-9.

Bum An, H., Jin Yu, M., Man Kim, J., Jin, M., Jeon, J.-K., Hoon Park, S., Kim, S.-S., & Park, Y.-K. (2012). *Indoor formaldehyde removal over CMK-3*. https://doi.org/10.1186/1556-276X-7-7

Bum An, H., Jin Yu, M., Man Kim, J., Jin, M., Jeon, J.-K., Hoon Park, S., Kim, S.-S., & Park, Y.-K. (2012). *Indoor formaldehyde removal over CMK-3*. https://doi.org/10.1186/1556-276X-7-7

Cai, Q., Luo, Z.-S., Pang, W.-Q., Fan, Y.-W., Chen, X.-H., & Cui, F.-Z. (2001). Dilute Solution Routes to Various Controllable Morphologies of MCM-41 Silica with a Basic Medium †. *Chemistry of Materials*, *13*(2), 258–263. https://doi.org/10.1021/cm990661z

Chen, H., & Wang, Y. (2002). Preparation of MCM-41 with high thermal stability and complementary textural porosity. Ceramics International, 28(5), 541-547.

Dahane, S., Galera, M. M., Marchionni, M., Viciana, M. S., Derdour, A., & García, M. G. (2016). Mesoporous silica based MCM-41 as solid-phase extraction sorbent combined with micro-liquid chromatography–quadrupole-mass spectrometry for the analysis of pharmaceuticals in waters. Talanta, 152, 378-391.

Dekker, C. (2007). Solid-state nanopores. In *Nature Nanotechnology* (Vol. 2, Issue 4, pp. 209–215). Nature Publishing Group. https://doi.org/10.1038/nnano.2007.27

Depeursinge, A., Racoceanu, D., Iavindrasana, J., Cohen, G., Platon, A., Poletti, P.-A., & Muller, H. (2010). Fusing Visual and Clinical Information for Lung Tissue Classification in HRCT Data. *Artificial Intelligence in Medicine*, 1118. https://doi.org/10.1016/j

Dingler, F. A., Wang, M., Mu, A., Millington, C. L., Oberbeck, N., Watcham, S., . . . Patel, K. J. (2020). Two Aldehyde Clearance Systems Are Essential to Prevent Lethal Formaldehyde Accumulation in Mice and Humans. Molecular Cell. doi:https://doi.org/10.1016/j.molcel.2020.10.012

Duong, A., Steinmaus, C., McHale, C. M., Vaughan, C. P., & Zhang, L. (2011). Reproductive and developmental toxicity of formaldehyde: A systematic review. In *Mutation Research - Reviews in Mutation Research* (Vol. 728, Issue 3, pp. 118–138). Elsevier. https://doi.org/10.1016/j.mrrev.2011.07.003

Ebnesajjad, S. (2014). Surface Treatment and Bonding of Ceramics. In *Surface Treatment of Materials for Adhesive Bonding* (pp. 283–299). Elsevier. https://doi.org/10.1016/b978-0-323-26435-8.00011-3

Ewlad-Ahmed, A. M., Morris, M. A., Patwardhan, S. V., & Gibson, L. T. (2012). Removal of formaldehyde from air using functionalized silica supports. *Environmental Science and Technology*, *46*(24), 13354–13360. https://doi.org/10.1021/es303886q

Fadeel, B., & Garcia-Bennett, A. E. (2010). Better safe than sorry: Understanding the toxicological properties of inorganic nanoparticles manufactured for biomedical applications. *Advanced Drug Delivery Reviews*, *62*(3), 362–374. https://doi.org/10.1016/j.addr.2009.11.008

Feng, Y., Panwar, N., Tng, D. J. H., Tjin, S. C., Wang, K., & Yong, K. T. (2016). The application of mesoporous silica nanoparticle family in cancer theranostics. In *Coordination Chemistry Reviews* (Vol. 319, pp. 86–109). Elsevier. https://doi.org/10.1016/j.ccr.2016.04.019

Formaldehyde and Cancer Risk - National Cancer Institute. (n.d.). Retrieved October 6,2020,from https://www.cancer.gov/aboutcancer/causesprevention/risk/substances/formaldehyde/formaldehyde-fact-sheet

Formaldehyde What is formaldehyde? - Google Search. (n.d.). Retrieved September 7, 2020, from https://www.google.com/search?q=FormaldehydeWhat+is+formaldehyde%3F&oq=FormaldehydeWhat+is+formaldehyde%3F&aqs=chrome.69i57&sourceid=chrome&ie=UTF-8

Fowler, C. E., Khushalani, D., Lebeau, B., & Mann, S. (2001). Nanoscale materials with mesostructured interiors. *Advanced Materials*, *13*(9), 649–652. https://doi.org/10.1002/1521-4095(200105)13:9<649::AID-ADMA649>3.0.CO;2-G

Fox, C. H., Johnson, F. B., Whiting, J., & Roller, P. P. (1985). Formaldehyde fixation. Journal of Histochemistry & Cytochemistry, 33(8), 845-853.

Gesser, H. D. (1984). The reduction of indoor formaldehyde gas and that emanating from urea formaldehyde foam insulation (UFFI). *Environment International*, *10*(4), 305–307. https://doi.org/10.1016/0160-4120(84)90136-3

Golden, R. (2011). Identifying an indoor air exposure limit for formaldehyde considering both irritation and cancer hazards. In Critical Reviews in Toxicology (Vol. 41, Issue 8, pp. 672–721). Taylor & Francis. https://doi.org/10.3109/10408444.2011.573467

Greasley, S. L., Page, S. J., Sirovica, S., Chen, S., Martin, R. A., Riveiro, A., Hanna, J. V., Porter, A. E., & Jones, J. R. (2016). Controlling particle size in the Stöber process and incorporation of calcium. *Journal of Colloid and Interface Science*, *469*, 213–223. https://doi.org/10.1016/j.jcis.2016.01.065

Grosso, D., Babonneau, F., Albouy, P. A., Amenitsch, H., Balkenende, A. R., Brunet-Bruneau, A., & Rivory, J. (2002). An in situ study of mesostructured CTAB-silica film formation during dip coating using time-resolved SAXS and interferometry measurements. *Chemistry of Materials*, *14*(2), 931–939. https://doi.org/10.1021/cm011255u

Gürü, M., Tekeli, S., & Bilici, I. (2006). Manufacturing of urea-formaldehyde-based composite particleboard from almond shell. *Materials and Design*, *27*(10), 1148–1151. https://doi.org/10.1016/j.matdes.2005.03.003

Gutwein, L. G., & Webster, T. J. (2004). Increased viable osteoblast density in the presence of nanophase compared to conventional alumina and titania particles. *Biomaterials*, *25*(18), 4175–4183. https://doi.org/10.1016/j.biomaterials.2003.10.090

Halvarsson, S., Edlund, H., & Norgren, M. (2008). Properties of medium-density fibreboard (MDF) based on wheat straw and melamine modified urea formaldehyde (UMF) resin. *Industrial Crops and Products*, *28*(1), 37–46. https://doi.org/10.1016/j.indcrop.2008.01.005

Harmer, M. A., Farneth, W. E., & Sun, Q. (1996). High surface area nafion resin/silica nanocomposites: A new class of solid acid catalyst. *Journal of the American Chemical Society*, *118*(33), 7708–7715. https://doi.org/10.1021/ja9541950

Hartmann, M., & Bischof, C. (1999). Mechanical stability of mesoporous molecular sieve MCM-48 studied by adsorption of benzene, n-heptane, and cyclohexane. *Journal of Physical Chemistry B*, *103*(30), 6230–6235. https://doi.org/10.1021/jp991103a

Hartmann, M., & Bischof, C. (1999). Mechanical stability of mesoporous molecular sieve MCM-48 studied by adsorption of benzene, n-heptane, and cyclohexane. *Journal of Physical Chemistry B*, *103*(30), 6230–6235. https://doi.org/10.1021/jp991103a

Heck, D. A., Casanova, M., & Starr, T. B. (1990). Formaldehyde toxicity-new understanding. *Critical Reviews in Toxicology*, *20*(6), 397–426. https://doi.org/10.3109/10408449009029329

Hemmilä, V., Zabka, M., & Adamopoulos, S. (2018). Evaluation of Dynamic Microchamber as a Quick Factory Formaldehyde Emission Control Method for Industrial Particleboards. *Advances in Materials Science and Engineering, 2018*. https://doi.org/10.1155/2018/4582383

Huang, H., Huang, H., Hu, P., Ye, X., & Leung, D. Y. C. (2013). Removal of formaldehyde using highly active Pt/TiO2 Catalysts without Irradiation. *International Journal of Photoenergy, 2013*. https://doi.org/10.1155/2013/350570

IARC Monographs on the Evaluation of Carcinogenic Risks to Humans Tobacco Smoke and Involuntary Smoking. (2004). http://monographs.iarc.fr/

Idris, S. A., Robertson, C., Morris, M. A., & Gibson, L. T. (2010). A comparative study of selected sorbents for sampling of aromatic VOCs from indoor air. *Analytical Methods*, *2*(11), 1803–1809. https://doi.org/10.1039/c0ay00418a

Kaden, D. A., Mandin, C., Nielsen, G. D., & Wolkoff, P. (2010). *Formaldehyde*. https://www.ncbi.nlm.nih.gov/books/NBK138711/

Kang, T., Jang, I., & Oh, S. G. (2016). Surface modification of silica nanoparticles using phenyl trimethoxy silane and their dispersion stability in N-methyl-2-pyrrolidone. *Colloids and Surfaces A: Physicochemical and Engineering Aspects*, *501*, 24–31. https://doi.org/10.1016/j.colsurfa.2016.04.060

Kang, T., Jang, I., & Oh, S. G. (2016). Surface modification of silica nanoparticles using phenyl trimethoxy silane and their dispersion stability in N-methyl-2-pyrrolidone. *Colloids and Surfaces A: Physicochemical and Engineering Aspects*, *501*, 24–31. https://doi.org/10.1016/j.colsurfa.2016.04.060

Kerkhof, O., Argiles, G., Brunet, D., Verines-Jouin, L., Solal, C., & Fiore, K. (2020). Études des alternatives potentielles au formaldéhyde en thanatopraxie. Archives des Maladies Professionnelles et de l'Environnement, 81(5), 696. doi:https://doi.org/10.1016/j.admp.2020.03.690

Kim, S. (2009). Environment-friendly adhesives for surface bonding of wood-based flooring using natural tannin to reduce formaldehyde and TVOC emission. *Bioresource Technology*, *100*(2), 744–748. https://doi.org/10.1016/j.biortech.2008.06.062

Kim, S., Kim, E., Kim, S., & Kim, W. (2004). *Surface Modification of Silica Nanoparticles by UV-Induced Graft Polymerization of Methyl Methacrylate*.

The Society of Chemical Engineers, Japan. https://doi.org/10.11491/APCCHE.2004.0.644.0

Kirik, S. D., Parfenov, V. A., & Zharkov, S. M. (2014). Monitoring MCM-41 synthesis by X-ray mesostructure analysis. Microporous and mesoporous materials, 195, 21-30.

Kosuge, K., Kubo, S., Kikukawa, N., & Takemori, M. (2007). Effect of pore structure in mesoporous silicas on VOC dynamic adsorption/desorption performance. *Langmuir*, *23*(6), 3095–3102. https://doi.org/10.1021/la062616t

Krishnamurthy, A., Thakkar, H., Rownaghi, A. A., & Rezaei, F. (2018). Adsorptive Removal of Formaldehyde from Air Using Mixed-Metal Oxides. *Industrial and Engineering Chemistry Research*, *57*(38), 12916–12925. https://doi.org/10.1021/acs.iecr.8b02962

Krishnamurthy, A., Thakkar, H., Rownaghi, A. A., & Rezaei, F. (2018). Adsorptive Removal of Formaldehyde from Air Using Mixed-Metal Oxides. *Industrial and Engineering Chemistry Research*, *57*(38), 12916–12925. https://doi.org/10.1021/acs.iecr.8b02962

Krishnamurthy, A., Thakkar, H., Rownaghi, A. A., & Rezaei, F. (2018). Adsorptive Removal of Formaldehyde from Air Using Mixed-Metal Oxides. *Industrial & Engineering Chemistry Research*, *57*(38), 12916–12925. https://doi.org/10.1021/acs.iecr.8b02962

Kumaravel, S., Wu, S.-H., Chen, G.-Z., Huang, S.-T., Lin, C.-M., Lee, Y.-C., & Chen, C.-H. (2021). Development of ratiometric electrochemical molecular switches to assay endogenous formaldehyde in live cells, whole blood and creatinine in saliva. Biosensors and Bioelectronics, 171, 112720. doi:https://doi.org/10.1016/j.bios.2020.112720

Latief, F. H., Chafidz, A., Junaedi, H., Alfozan, A., & Khan, R. (2019). Effect of alumina contents on the physicomechanical properties of alumina (Al2 o3) reinforced polyester composites. *Advances in Polymer Technology, 2019*. https://doi.org/10.1155/2019/5173537

Leaderer, B. P., & Hammond, S. K. (1991). Evaluation of Vapor-Phase Nicotine and Respirable Suspended Particle Mass as Markers for Environmental Tobacco Smoke. *Environmental Science and Technology*, *25*(4), 770–777. https://doi.org/10.1021/es00016a023

Li, X.-J., Fu, Q.-F., Zhang, Q.-H., Jiang, X.-M., Yang, F.-Q., Wei, W.-L., & Xia, Z.-N. (2015). Layer-by-layer self-assembly of polydopamine/gold nanoparticle/thiol coating as the stationary phase for open tubular capillary electrochromatography. Analytical Methods, 7(19), 8227-8234.

Liberman, A., Mendez, N., Trogler, W. C., & Kummel, A. C. (2014). Synthesis and surface functionalization of silica nanoparticles for nanomedicine. In *Surface Science Reports* (Vol. 69, Issues 2–3, pp. 132–158). Elsevier. https://doi.org/10.1016/j.surfrep.2014.07.001

Lin, Y. S., Hurley, K. R., & Haynes, C. L. (2012). Critical considerations in the biomedical use of mesoporous silica nanoparticles. In *Journal of Physical Chemistry Letters* (Vol. 3, Issue 3, pp. 364–374). UTC. https://doi.org/10.1021/jz2013837

Liu, P. S., & Chen, G. F. (2014). General Introduction to Porous Materials. In *Porous Materials* (pp. 1–20). Elsevier. https://doi.org/10.1016/B978-0-12-407788-1.00001-0

Ma, X. kun, Lee, N. H., Oh, H. J., Kim, J. W., Rhee, C. K., Park, K. S., & Kim, S. J. (2010). Surface modification and characterization of highly dispersed silica nanoparticles by a cationic surfactant. *Colloids and Surfaces A: Physicochemical and Engineering Aspects*, *358*(1–3), 172–176. https://doi.org/10.1016/j.colsurfa.2010.01.051

Marchand, C., Bulliot, B., Le Calvé, S., & Mirabel, P. (2006). Aldehyde measurements in indoor environments in Strasbourg (France). *Atmospheric Environment*, *40*(7), 1336–1345. https://doi.org/10.1016/j.atmosenv.2005.10.027

Maszara, W. P., Goetz, G., Caviglia, A., & McKitterick, J. B. (1988). Bonding of silicon wafers for silicon-on-insulator. *Journal of Applied Physics*, *64*(10), 4943–4950. https://doi.org/10.1063/1.342443

Matsumoto, A., Misran, H., & Tsutsumi, K. (2004). Adsorption characteristics of organosilica based mesoporous materials. *Langmuir*, *20*(17), 7139–7145. https://doi.org/10.1021/la0360409

Mehmood, A. (2017). *Mesoporous Silica Nanoparticles: A Review*. https://doi.org/10.4172/2329-6631.1000174

Meléndez-Ortiz, H., García-Cerda, L., Olivares-Maldonado, Y., Castruita, G., Mercado-Silva, J., & Perera-Mercado, Y. (2012). Preparation of spherical MCM-41 molecular sieve at room temperature: Influence of the synthesis

conditions in the structural properties. Ceramics International, 38(8), 6353-6358.

Meyer, C. D., Joiner, C. S., & Stoddart, J. F. (2007). Template-directed synthesis employing reversible imine bond formation. Chemical Society Reviews, 36(11), 1705-1723.

Morris, J. K. (1965). A formaldehyde glutaraldehyde fixative of high osmolality for use in electron microscopy. J. cell Biol, 27, 1A-149A.

Nanomaterials definition matters. (2019). In *Nature Nanotechnology* (Vol. 14, Issue 3, p. 193). Nature Publishing Group. https://doi.org/10.1038/s41565-019-0412-3

Nishiyabu, K. (2012). Powder space holder metal injection molding (PSH-MIM) of micro-porous metals. In *Handbook of Metal Injection Molding* (pp. 349–390). Elsevier Inc. https://doi.org/10.1533/9780857096234.3.349

Obrey, S. J., & Barron, A. R. (2002). A chemically functionalized carboxylate-alumoxane nanoparticle support for olefin polymerization catalysts. *Macromolecules*, *35*(5), 1499–1503. https://doi.org/10.1021/ma010314m

Ongwandee, M., Moonrinta, R., Panyametheekul, S., Tangbanluekal, C., & Morrison, G. (2009). Concentrations and strengths of formaldehyde and acetaldehyde in office buildings in Bangkok, Thailand. *Indoor and Built Environment*, *18*(6), 569–575. https://doi.org/10.1177/1420326X09349897

OSHA Fact Sheet: Formaldehyde | Occupational Safety and Health Administration. (n.d.). Retrieved October 6, 2020, from https://www.osha.gov/OshDoc/data_General_Facts/formaldehyde-factsheet.html

OSHA rulemaking on formaldehyde exposure limits | Occupational Safety and Health Administration. (n.d.). Retrieved November 13, 2020, from https://www.osha.gov/laws-regs/standardinterpretations/1998-03-13-0?fbclid=IwAR0P0JB-lSpO6g8COS-9HHcvh4TYa5rNxd7mKhMLyKghV2wddxtOP6XCNEw

Park, J. T., Seo, J. A., Ahn, S. H., Kim, J. H., & Kang, S. W. (2010). Surface modification of silica nanoparticles with hydrophilic polymers. *Journal of Industrial and Engineering Chemistry*, *16*(4), 517–522. https://doi.org/10.1016/j.jiec.2010.03.030

Pauling, L. (1932). The nature of the chemical bond. IV. The energy of single bonds and the relative electronegativity of atoms. Journal of the American Chemical Society, 54(9), 3570-3582.

Prado, Ó. J., Veiga, M. C., & Kennes, C. (n.d.). *Removal of formaldehyde, methanol, dimethylether and carbon monoxide from waste gases of synthetic resin-producing industries*. https://doi.org/10.1016/j.chemosphere.2007.09.039

Qu, M., Lu, J., & He, R. (2017). Formaldehyde from environment. In *Formaldehyde and Cognition* (pp. 1–19). Springer Netherlands. https://doi.org/10.1007/978-94-024-1177-5_1

Rešković, S., Brlić, T., Jakovljević, S., & Jandrlić, I. (2017). Surface contamination of alumina ceramics by carbon. Engineering Review, 37, 335-340.

Rouquerol, J., Avnir, D., Fairbridge, C. W., Everett, D. H., Haynes, J. M., Pernicone, N., Ramsay, J. D. F., Sing, K. S. W., & Unger, K. K. (1994). Recommendations for the characterization of porous solids (Technical Report). *Pure and Applied Chemistry*, *66*(8), 1739–1758. https://doi.org/10.1351/pac199466081739

Salem, M. Z. M., Böhm, M., Beránková, J., & Srba, J. (2011). Effect of some manufacturing variables on formaldehyde release from particleboard: Relationship between different test methods. *Building and Environment*, *46*(10), 1946–1953. https://doi.org/10.1016/j.buildenv.2011.04.004

Salthammer, T., Mentese, S., & Marutzky, R. (n.d.). *Formaldehyde in the Indoor Environment*. https://doi.org/10.1021/cr800399g

Schmidt, J., Altun, A. A., Schwentenwein, M., & Colombo, P. (2019). Complex mullite structures fabricated via digital light processing of a preceramic polysiloxane with active alumina fillers. *Journal of the European Ceramic Society*, *39*(4), 1336–1343. https://doi.org/10.1016/j.jeurceramsoc.2018.11.038

Smitha, S., Shajesh, P., Mukundan, P., Nair, T. D. R., & Warrier, K. G. K. (2007). Synthesis of biocompatible hydrophobic silica-gelatin nano-hybrid by sol-gel process. *Colloids and Surfaces B: Biointerfaces*, *55*(1), 38–43. https://doi.org/10.1016/j.colsurfb.2006.11.008

Srisuda, S., & Virote, B. (2008). Adsorption of formaldehyde vapor by amine-functionalized mesoporous silica materials. Journal of Environmental Sciences, 20(3), 379-384.

Stein, A. (2003). Advances in microporous and mesoporous solids - Highlights of recent progress. *Advanced Materials*, *15*(10), 763–775. https://doi.org/10.1002/adma.200300007

Swain, C. G., Powell, A. L., Sheppard, W. A., & Morgan, C. R. (1979). Mechanism of the Cannizzaro reaction. Journal of the American Chemical Society, 101(13), 3576-3583.

Tan, H., Chen, D., Li, N., Xu, Q., Li, H., He, J., & Lu, J. (2019). Platinum-Supported Zirconia Nanotube Arrays Supported on Graphene Aerogels Modified with Metal–Organic Frameworks: Adsorption and Oxidation of Formaldehyde at Room Temperature. *Chemistry – A European Journal*, *25*(72), 16718–16724. https://doi.org/10.1002/chem.201904426

Teiri, H., Pourzamzni, H., & Hajizadeh, Y. (2018). Phytoremediation of formaldehyde from indoor environment by ornamental plants: An approach to promote occupants health. *International Journal of Preventive Medicine*, *9*(1), 70. https://doi.org/10.4103/ijpvm.IJPVM_269_16

Trouvé, A., Batonneau-Gener, I., Valange, S., Bonne, M., & Mignard, S. (2012). Tuning the hydrophobicity of mesoporous silica materials for the adsorption of organic pollutant in aqueous solution. Journal of hazardous materials, 201, 107-114.

Ueno, Y., Horiuchi, T., Tomita, M., Niwa, O., Zhou, H. shen, Yamada, T., & Honma, I. (2002). Separate detection of BTX mixture gas by a microfluidic device using a function of nanosized pores of mesoporous silica adsorbent. *Analytical Chemistry*, *74*(20), 5257–5262. https://doi.org/10.1021/ac0201732

Vazquez, N. I., Gonzalez, Z., Ferrari, B., & Castro, Y. (2017). Synthesis of mesoporous silica nanoparticles by sol–gel as nanocontainer for future drug delivery applications. Boletín de la Sociedad Española de Cerámica y Vidrio, 56(3), 139-145.

Vickers, N. J. (2017). Animal Communication: When I'm Calling You, Will You Answer Too? In *Current Biology* (Vol. 27, Issue 14, pp. R713–R715). Cell Press. https://doi.org/10.1016/j.cub.2017.05.064

Wang, X., Wang, P., Jiang, Y., Su, Q., & Zheng, J. (2014). Facile surface modification of silica nanoparticles with a combination of noncovalent and covalent methods for composites application. *Composites Science and Technology*, *104*, 1–8. https://doi.org/10.1016/j.compscitech.2014.08.027

Yang, P., Gai, S., & Lin, J. (2012). Functionalized mesoporous silica materials for controlled drug delivery. *Chemical Society Reviews*, *41*(9), 3679–3698. https://doi.org/10.1039/c2cs15308d

Zdravkov, B. D., Čermák, J. J., Šefara, M., & Janků, J. (2007). Pore classification in the characterization of porous materials: A perspective. *Central European Journal of Chemistry*, *5*(2), 385–395. https://doi.org/10.2478/s11532-007-0017-9

Zhang, D., Zhang, M., Ding, F., Liu, W., Zhang, L., & Cui, L. (2020). Efficient removal of formaldehyde by polyethyleneimine modified activated carbon in a fixed bed. *Environmental Science and Pollution Research*, *27*(15), 18109–18116. https://doi.org/10.1007/s11356-020-08019-5

Zou, H., Wu, S., & Shen, J. (2008). Polymer/Silica Nanocomposites: Preparation, characterization, propertles, and applications. In *Chemical Reviews* (Vol. 108, Issue 9, pp. 3893–3957). American Chemical Society. https://doi.org/10.1021/cr068035q

APPENDICES

APPENDIX A

Amine Functionalized Mesoporous Silica Characterization

Table A1 Particle Size analysis of FESEM image of MPS1, MPS2 and MPS3

	Particle Sizes (µm)		
	MPS1	**MPS2**	**MPS3**
	0.8306	0.5571	0.7075
	0.7425	0.6059	0.4669
	0.8542	0.3791	0.5409
	0.3404	0.4844	0.4597
	0.8005	0.5791	0.549
	0.8802	0.447	0.5558
	0.6528	0.8679	0.5275
	0.9513	0.5089	0.486
	0.9559	0.5762	0.5576
	1.1177	0.6368	0.8293
	0.6218	0.5703	0.4322
	0.4943	0.5519	0.7813
	0.6938	0.626	0.7785
	0.9445	0.5838	0.4955
	0.9288	1.2188	0.5204
	0.6443	0.6382	0.3661
	0.4814	0.4281	0.5018
	0.3265	0.668	0.5719
	0.2917	0.8223	0.2954
	0.258	0.7747	0.3185
	0.8984	0.6023	0.5685
	1.0013	0.4161	0.6765
	0.809	0.5162	0.7598
	0.6957	0.6331	0.7865
	1.1501	0.5604	0.4598
	1.0075	0.8389	0.4872
	0.709	0.8685	0.4557
	0.6929	0.4998	0.5678
	0.6788	0.2531	0.4674
	0.4862	0.4209	0.6389
	0.9573	0.4729	0.3977
	1.1387	0.4301	0.7642
	0.2929	0.6119	0.7306
	0.9539	0.5615	0.2951
	0.8808	0.4708	0.4914
Average Particle Size (µm)	0.72	0.58	0.55
Standard Deviation	0.26	0.17	0.16

Table A2 Particle Size of FESEM image AMPS1, AMPS2 and AMPS3

	Particle Size (µm)		
	AMPS1	**AMPS2**	**AMPS3**
	0.5955	0.6405	0.4169
	0.5909	0.6656	0.6799
	0.4039	0.6948	0.6298
	0.6874	0.6804	0.5213
	0.5754	0.6023	0.5161
	0.5706	0.4501	0.4379
	0.6414	0.5376	0.4691
	0.526	0.6192	0.2455
	0.6551	0.6	0.5135
	0.5181	0.5359	0.4665
	0.5236	0.6587	0.5223
	0.6488	0.7433	0.6871
	0.4977	0.4278	0.8133
	0.5398	0.6235	0.5735
	0.6108	0.6155	0.5201
	0.3418	0.4683	0.6633
	0.4294	0.5946	0.7625
	0.5972	0.7082	0.5758
	0.471	0.5334	0.4417
	0.4721	0.4598	0.3466
	0.6607	0.6998	0.259
	0.3176	0.9559	0.3326
	0.2244	0.6759	0.2733
	0.8884	0.7724	0.9043
	0.4731	0.8607	0.3952
	0.4169	0.8235	0.5811
	0.5751	0.7382	0.5158
	0.4899	0.4817	0.5272
	0.6426	0.5708	0.5071
	0.7225	0.5365	0.6372
	0.5299	0.576	0.6913
	0.819	0.6863	0.932
	0.8387	0.6488	0.8004
	0.5769	0.9815	0.9658
	0.4109	0.6479	0.5619
	0.407	0.5551	0.6173
	0.6064	0.2977	0.3083
	0.7342	0.3132	0.7708
Average Particle Size (µm)	0.58	0.63	0.55
Standard Deviation	0.15	0.17	0.17

Table A3 N_2 adsorption desorption data of MPS3

MPS3 - Adsorption		MPS3 - Desorption	
Relative Pressure (P/Po)	**Quantity Adsorbed (cm^3/g STP)**	**Relative Pressure (P/Po)**	**Quantity Adsorbed (cm^3/g STP)**
0.025967	166.2761	0.991521	408.3352
0.049113	186.8645	0.962113	397.0485
0.078307	205.6993	0.933052	393.3825
0.097036	216.4088	0.907134	391.4538
0.122741	231.1344	0.881953	390.1011
0.146974	246.1455	0.85683	389.0355
0.170842	263.0558	0.831702	388.1406
0.194544	281.877	0.825413	387.8349
0.218566	301.8361	0.800343	386.9836
0.243653	321.5425	0.775517	386.3297
0.270193	339.0639	0.750545	385.6022
0.297798	352.7972	0.725421	384.8787
0.326418	362.2936	0.700477	384.1474
0.348883	367.2986	0.675484	383.4877
0.374326	371.0852	0.650546	382.804
0.399683	373.6335	0.625516	382.1215
0.424824	375.4092	0.600501	381.2775
0.449954	376.7551	0.575464	380.5084
0.475015	377.8396	0.550539	379.7574
0.500039	378.7525	0.52558	379.0984
0.525073	379.5135	0.500653	378.2006
0.550031	380.2504	0.47555	377.2165
0.575041	381.0115	0.450558	376.2684
0.600201	381.6703	0.425814	375.2298
0.625109	382.2976	0.401094	373.2377
0.65016	382.9414	0.375953	370.409
0.675067	383.5931	0.35133	366.8142
0.700144	383.9513	0.326645	361.546
0.743643	385.0092	0.302186	353.6854
0.750209	385.2569	0.277592	342.41
0.775215	385.8798	0.25315	327.4642
0.799775	386.5878	0.228345	308.8908
0.824937	387.374	0.20336	288.0991
0.849918	388.2276	0.178078	267.2184
0.874942	389.1471	0.153019	248.5644
0.899797	390.2658	0.127633	232.1174
0.924735	391.7656	0.102297	217.2599
0.949507	393.9767	0.077201	202.8135
0.97373	398.2509	0.052304	186.7358
0.991521	408.3352	0.025875	163.4493

Table A4 BJH pore size distribution data of MPS3

Pore Diameter (nm)	dV/dlog(D) Pore Volume (cm^3/g)
60.83603	0.030807
35.75435	0.027416
25.02766	0.0256
19.41329	0.02478
15.88553	0.024449
13.44023	0.024647
12.32915	0.039577
11.26397	0.029077
9.971471	0.024677
8.937276	0.032193
8.084233	0.035756
7.372137	0.04064
6.768031	0.039063
6.247418	0.044708
5.792772	0.047922
5.391551	0.067137
5.034653	0.063202
4.715289	0.064979
4.42713	0.05703
4.165065	0.089899
3.924492	0.103517
3.702982	0.101927
3.499555	0.118876
3.311243	0.266941
3.133631	0.393966
2.967465	0.529413
2.811869	0.80706
2.664824	1.257136
2.524756	1.828241
2.390627	2.451792
2.260624	2.971634
2.133198	3.19694
2.007459	2.962106
1.88347	2.350083
1.759236	1.660998

Table A5 N_2 adsorption desorption data of AMPS3

AMPS1 - Adsorption		AMPS1 - Desorption	
Relative Pressure (P/Po)	**Quantity Adsorbed (cm^3/g STP)**	**Relative Pressure (P/Po)**	**Quantity Adsorbed (cm^3/g STP)**
0.023891	163.985	0.992775	429.697
0.048854	187.4272	0.960579	420.1672
0.07841	207.9235	0.932784	416.939
0.096625	220.2399	0.907157	415.0333
0.121624	239.1052	0.881988	413.4958
0.145966	258.9475	0.875484	413.035
0.17185	276.2631	0.850328	411.9146
0.199402	288.1676	0.825711	410.7909
0.22639	296.068	0.800639	409.6121
0.252514	302.1545	0.77566	408.4517
0.276416	307.1555	0.750595	407.2442
0.300636	311.8625	0.725687	405.9272
0.325221	316.4024	0.700668	404.6038
0.350237	320.821	0.675738	403.2067
0.374529	324.9563	0.650694	401.8575
0.399495	329.3047	0.62572	400.3794
0.424636	333.6451	0.600745	398.831
0.449483	338.0034	0.575639	397.2361
0.474441	342.5813	0.550712	395.6511
0.499501	347.2875	0.525928	393.9959
0.52446	352.0053	0.500874	392.1331
0.549282	357.0311	0.47728	387.9337
0.574373	362.2457	0.455996	356.7146
0.59922	367.61	0.427811	338.3114
0.624222	373.2882	0.386228	327.3817
0.649387	378.8724	0.358127	322.2603
0.674178	384.5142	0.333063	317.7143
0.699294	389.9735	0.325527	316.3674
0.724199	395.2127	0.301177	311.8034
0.749425	400.1613	0.276186	306.9722
0.774752	404.246	0.25122	301.6094
0.799634	407.3108	0.226393	295.7777
0.824826	409.6283	0.201525	288.524
0.849812	411.3359	0.177223	278.6793
0.874842	412.6443	0.153298	264.1104
0.899779	414.1564	0.128214	244.0288
0.924978	415.845	0.102354	223.6394
0.949637	418.0271	0.076641	205.8044
0.974207	421.7274	0.052379	188.9315
0.992775	429.697	0.026041	165.1212

Table A6 BJH pore size distribution data of AMPS3

Pore Diameter (nm)	dV/dlog(D) Pore Volume (cm^3/g)
57.5443	0.023063
35.46609	0.025835
25.00771	0.025866
19.41858	0.028859
17.22232	0.039791
15.17334	0.027528
12.9474	0.03458
11.28131	0.04233
9.981073	0.04826
8.94065	0.05713
8.08957	0.071098
7.377993	0.078378
6.773102	0.091488
6.251217	0.094337
5.795818	0.113203
5.394965	0.127316
5.037441	0.138535
4.717404	0.145636
4.430088	0.161603
4.16786	0.19161
3.934146	0.540605
3.735041	5.007959
3.527615	2.157181
3.25634	0.715297
3.022178	0.392275
2.852613	0.389582
2.756486	0.372233
2.658652	0.412173
2.517898	0.430148
2.381521	0.511263
2.250555	0.577311
2.123681	0.79519
2.001144	1.237268
1.882489	2.015666
1.761494	2.609352

APPENDIX B

Formaldehyde Decay and Adsorption Capacity of the Synthesized Samples

Table B1 Formaldehyde decay value of Powder samples with time

Time (mins)	Decay of 0.5g of Powder Samples at 3 ppm HCHO Concentrations			
	MPS	**AMPS1**	**AMPS2**	**AMPS3**
0	1.0000	1.0000	1.0000	1.0000
1	0.9655	0.9684	0.9684	0.9684
2	0.9425	0.9368	0.9368	0.9474
3	0.9310	0.9263	0.9263	0.9263
4	0.9195	0.9158	0.9158	0.9158
5	0.9080	0.9053	0.9053	0.9053
6	0.8966	0.8947	0.8947	0.8947
7	0.8851	0.8842	0.8842	0.8842
8	0.8736	0.8737	0.8737	0.8737
9	0.8621	0.8632	0.8632	0.8632
10	0.8506	0.8526	0.8526	0.8526
11	0.8391	0.8421	0.8421	0.8421
12	0.8391	0.8316	0.8316	0.8421
13	0.8276	0.8211	0.8211	0.8316
14	0.8276	0.8105	0.8105	0.8316
15	0.8161	0.8105	0.8105	0.8211
20	0.7931	0.8000	0.7895	0.7684
25	0.7701	0.7789	0.7684	0.7158
30	0.7471	0.7579	0.7474	0.6737
45	0.7011	0.7053	0.6947	0.5895
60	0.6552	0.6632	0.6421	0.5263
75	0.6207	0.6316	0.6000	0.4947
90	0.5977	0.6000	0.5684	0.4526
105	0.5747	0.5684	0.5474	0.4211
120	0.5517	0.5474	0.5263	0.4000

Table B2 Formaldehyde decay value of AMPS3 at 3 ppm, 6 ppm, 9 ppm and 12 ppm formaldehyde concentrations

Time (mins)	HCHO decay at different concentration			
	3ppm	6ppm	9ppm	12ppm
0	1	1	1	1
1	0.968421	0.964029	0.929412	0.985965
2	0.947368	0.935252	0.864706	0.978947
3	0.926316	0.913669	0.811765	0.961403
4	0.915789	0.884892	0.764706	0.950877
5	0.905263	0.863309	0.723529	0.940351
6	0.894737	0.841727	0.688235	0.933333
7	0.884211	0.820144	0.652941	0.922807
8	0.873684	0.798561	0.629412	0.91228
9	0.863158	0.776978	0.611765	0.905263
10	0.852632	0.755396	0.588235	0.894737
11	0.842105	0.733813	0.582353	0.887719
12	0.842105	0.71223	0.576471	0.880701
13	0.831579	0.705036	0.570588	0.870175
14	0.831579	0.697842	0.564706	0.863158
15	0.821053	0.683453	0.558824	0.85614
20	0.768421	0.640288	0.541176	0.814035
25	0.715789	0.597122	0.529412	0.775438
30	0.673684	0.561151	0.517647	0.740351
45	0.589474	0.460432	0.470588	0.631579
60	0.526316	0.417266	0.435294	0.540351
75	0.494737	0.381295	0.4	0.449123
90	0.452632	0.359712	0.376471	0.382456
105	0.421053	0.352518	0.352941	0.364912
120	0.4	0.345324	0.335294	0.354386

Table B3 Formaldehyde adsorption capacity of AMPS3 at 3 ppm, 6 ppm, 9 ppm and 12 ppm formaldehyde concentrations

Time (mins)	Adsorption Capacity of AMPS3 at different time			
	3ppm	6ppm	9ppm	12ppm
0.00	0.00	0.00	0.00	0.00
1.00	2.82	4.71	11.30	3.77
2.00	4.71	8.47	21.66	5.65
3.00	6.59	11.30	30.13	10.36
4.00	7.53	15.07	37.66	13.18
5.00	8.47	17.89	44.26	16.01
6.00	9.42	20.72	49.91	17.89
7.00	10.36	23.54	55.56	20.72
8.00	11.30	26.37	59.32	23.54
9.00	12.24	29.19	62.15	25.42
10.00	13.18	32.01	65.91	28.25

Time (mins)	Adsorption Capacity of AMPS3 at different time			
	3ppm	6ppm	9ppm	12ppm
11.00	14.12	34.84	66.85	30.13
12.00	14.12	37.66	67.80	32.01
13.00	15.07	38.61	68.74	34.84
14.00	15.07	39.55	69.68	36.72
15.00	16.01	41.43	70.62	38.61
20.00	20.72	47.08	73.45	49.91
25.00	25.42	52.73	75.33	60.26
30.00	29.19	57.44	77.21	69.68
45.00	36.72	70.62	84.75	98.87
60.00	42.37	76.27	90.39	123.35
75.00	45.20	80.98	96.04	147.83
90.00	48.96	83.80	99.81	165.72
105.00	51.79	84.75	103.58	170.43
120.00	53.67	85.69	106.40	173.26